Acta Neuropathol (2016) 131:115–135
DOI 10.1007/s00401-015-1506-0

ORIGINAL PAPER

SNTF immunostaining reveals previously undetected axonal pathology in traumatic brain injury

Victoria E. Johnson[1] · William Stewart[1,2,3] · Maura T. Weber[1] · D. Kacy Cullen[1] · Robert Siman[1] · Douglas H. Smith[1]

Received: 19 June 2015 / Revised: 27 October 2015 / Accepted: 31 October 2015 / Published online: 20 November 2015

Abstract Diffuse axonal injury (DAI) is a common feature of severe traumatic brain injury (TBI) and may also be a predominant pathology in mild TBI or "concussion". The rapid deformation of white matter at the instant of trauma can lead to mechanical failure and calcium-dependent proteolysis of the axonal cytoskeleton in association with axonal transport interruption. Recently, a proteolytic fragment of alpha-II spectrin, "SNTF", was detected in serum acutely following mild TBI in patients and was prognostic for poor clinical outcome. However, direct evidence that this fragment is a marker of DAI has yet to be demonstrated in either humans following TBI or in models of mild TBI. Here, we used immunohistochemistry (IHC) to examine for SNTF in brain tissue following both severe and mild TBI. Human severe TBI cases (survival <7d; $n = 18$) were compared to age-matched controls ($n = 16$) from the Glasgow TBI archive. We also examined brains from an established model of mild TBI at 6, 48 and 72 h post-injury versus shams. IHC specific for SNTF was compared to that of amyloid precursor protein (APP), the current standard for DAI diagnosis, and other known markers of axonal pathology including non-phosphorylated neurofilament-H (SMI-32), neurofilament-68 (NF-68) and compacted neurofilament-medium (RMO-14) using double and triple immunofluorescent labeling. Supporting its use as a biomarker of DAI, SNTF immunoreactive axons were observed at all time points following both human severe TBI and in the model of mild TBI. Interestingly, SNTF revealed a subpopulation of degenerating axons, undetected by the gold-standard marker of transport interruption, APP. While there was greater axonal co-localization between SNTF and APP after severe TBI in humans, a subset of SNTF positive axons displayed no APP accumulation. Notably, some co-localization was observed between SNTF and the less abundant neurofilament subtype markers. Other SNTF positive axons, however, did not co-localize with any other markers. Similarly, RMO-14 and NF-68 positive axonal pathology existed independent of SNTF and APP. These data demonstrate that multiple pathological axonal phenotypes exist post-TBI and provide insight into a more comprehensive approach to the neuropathological assessment of DAI.

Keywords Traumatic brain injury · TBI · Concussion · Mild TBI · Diffuse axonal injury · Spectrin breakdown · SNTF · Axonal pathology · Amyloid precursor protein · Neurofilaments

Introduction

Traumatic brain injury (TBI) is recognized as a major public health problem, inflicting substantial burden on individuals, their families and economies worldwide [16, 18, 30, 32]. Moreover, emerging data describing persistent symptoms and the potential for chronic neurodegenerative

Electronic supplementary material The online version of this article (doi:10.1007/s00401-015-1506-0) contains supplementary material, which is available to authorized users.

✉ Douglas H. Smith
smithdou@upenn.edu

[1] Department of Neurosurgery, Penn Center for Brain Injury and Repair, Perelman School of Medicine, University of Pennsylvania, 105 Hayden Hall, 3320 Smith Walk, Philadelphia, PA 19104, USA

[2] Department of Neuropathology, Queen Elizabeth Glasgow University Hospital, Glasgow G51 4TF, UK

[3] University of Glasgow, Glasgow G12 8QQ, UK

consequences following repetitive mild TBI (mTBI) or "concussion" have ignited considerable public concern [71].

Axons are especially vulnerable to the mechanical loading of the brain during trauma, making diffuse axonal injury (DAI) one of the most common pathologies of TBI [1–3, 25, 35]. Specifically, rapid acceleration/deceleration caused by rotational forces at the moment of injury precipitates brain pathology via shear, tensile, and compressive strains [21, 43]. Although axons rarely disconnect at the time of head impact, even in severe TBI, the dynamic deformation of white matter can cause immediate or primary disruption of the axonal cytoskeleton [35, 78, 79]. In addition, multiple evolving neurochemical changes are induced by TBI, including rapid and progressive elevations in intra-axonal calcium [10, 33, 39, 50, 74, 80, 82]. At pathological levels, the calcium overload activates the calcium-dependent calpain proteases, which can in turn initiate catastrophic secondary damage to the axon [13, 36, 42, 56, 57, 68, 74, 80].

A well-characterized consequence of axonal cytoskeletal disruption is the interruption of axonal transport, leading to accumulation of transported proteins in axonal swellings. Indeed, visualization of the accumulation of amyloid precursor protein (APP) in damaged axons is the current gold-standard neuropathological approach for the diagnosis of DAI [23, 35, 59]. Interestingly, while all axons of a given white matter tract endure similar high strains and strain rates during TBI, only a subset of the total axonal population accumulates APP. This suggests that this putative marker of axonal pathology may not identify all injured axons at any given time post-TBI. Supporting this premise, previous work in rodents indicates that a marker for compacted neurofilament-medium (RMO-14) identifies injured axons that do not accumulate APP [77].

While DAI was largely thought to be a consequence of moderate or severe TBI, emerging evidence suggests that it may also be the predominant pathology of mild TBI [5–7, 40, 44, 81, 84]. In particular, advanced neuroimaging studies of mTBI patients consistently identify white matter changes, the extent of which appear to determine clinical outcome [17, 44, 45, 62]. In addition, following a swine model of head rotational acceleration scaled to human mTBI parameters, DAI was the most notable pathology [8].

Recent studies evaluating blood biomarkers have provided further evidence in support of axonal damage in mTBI. Specifically, elevations in the axon-enriched microtubule-associated protein tau have been demonstrated in the blood of professional ice hockey players with sports-related concussion [58]. In this same cohort, serum elevations of a proteolytic fragment of the axonal protein, spectrin, were detected and correlated with the severity of post-concussion symptoms [65]. In another mTBI cohort, acute serum levels of this same spectrin fragment identified patients who went on to have persisting neurocognitive dysfunction [62]. This blood biomarker is the 1176 residue calpain-derived alpha-II spectrin *N*-terminal fragment, or "SNTF", and its genesis likely reflects injury-induced elevations in intra-axonal calcium and activation of calpain [80].

While SNTF has been detected using Western blotting in brain tissue from severe TBI patients [41], the specific anatomical source of SNTF has yet to be demonstrated in humans following TBI of any severity or in any models of mTBI. Nonetheless, SNTF has been observed to accumulate in axons acutely after moderate to severe TBI in small animal models and with in vitro models of neuronal trauma [13, 42, 56, 57, 80]. Interestingly, SNTF has been demonstrated to co-localize with RMO-14 immunoreactivity indicating compacted neurofilaments in rodent models [13]. However, the relative role of SNTF as a marker of DAI when compared to the gold standard, APP, has not been explored. Moreover, potential co-localization with RMO-14 or other neurofilament subtypes has not been examined in humans or larger animal models of mTBI.

Here, we performed neuropathological examinations of SNTF immunostaining after mild and severe TBI. Since mild TBI in humans is rarely fatal, and thus tissue is unavailable for acute post-mortem analysis, we used a parallel approach of examining brain sections of single severe TBI in humans as well as from an established swine model of mild TBI. SNTF immunohistochemistry was compared to that of both APP and several neurofilament subtype markers of axonal pathology.

Methods

Non-impact rotational acceleration model of mild TBI in swine

All animal experiments were conducted in accordance with protocols approved by The University of Pennsylvania Institutional Animal Care and Use Committee. The University of Pennsylvania is accredited by the Association for Assessment and Accreditation of Laboratory Animal Care (AAALAC). Six-month-old female Hanford miniature swine (23–36 kg) were subjected to the established non-impact rotational acceleration model as described in detail previously [8, 43, 55, 69, 72]. Briefly, following induction using 0.4 mg/Kg midazolam IM and 5 % inhaled isoflurane, animals were intubated and anesthesia maintained via 2.5 % inhaled isoflurane. The HYGE pneumatic actuator device was then used to induce head rotation. Specifically, the HYGE actuator generates linear motion via the triggered release of pressurized nitrogen. This linear motion is then converted to angular motion via custom-designed

linkage assemblies to induce rotation of up to 110° within 20 ms. Rotational kinematics were recorded using angular velocity transducers (Applied Technology Associates, Albuquerque, NM) mounted to the linkage sidearm coupled to a National Instruments (Austin, TX) data acquisition system running custom LabView software (10 kHz sampling rate). In this fashion, we produced pure impulsive centroidal head rotation in the coronal plane with peak angular velocity of 207–247 rad/sec. Animals were recovered from anesthesia and returned to the housing facility. While the procedure is non-surgical, preemptive analgesia was provided post-injury in the form of 0.3 mg of buprenorphine (slow release preparation) SQ and acetaminophen 50 mg/Kg PR 6 hourly.

Animals were euthanized at 6 h ($n = 3$), 48 h ($n = 2$) and 72 h ($n = 3$) post-injury and compared to sham animals ($n = 3$) euthanized at 72 h post-sham-injury. Specifically, all animals were deeply anesthetized and transcardially perfused using heparinized saline (4 L) followed by 10 % neutral buffered formalin (NBF) (8 L). The brain was subsequently removed and post-fixed for 7 days in 3 L of 10 % NBF. The whole brain was dissected into 5 mm blocks in the coronal plane and processed to paraffin using standard techniques.

Human post-mortem acute severe TBI cohort: demographic and clinical data

All tissue was obtained from the Glasgow TBI archive, Department of Neuropathology, Queen Elizabeth University Hospital, Glasgow, UK. Tissue was acquired at routine diagnostic autopsy and approval for use was granted by the NHS Greater Glasgow and Clyde Bio-repository Governance Committee. For this type of study, formal consent is not required.

TBI cases were selected to include patients who died acutely following severe TBI, with survival times ranging from 6 h to 1 week (median 1.5 days; $n = 18$). Detailed reports from the diagnostic autopsy and/or forensic reports were available for all cases and indicated a history of a single severe TBI, supported by autopsy findings. TBI cases were compared to material from age/sex-matched controls ($n = 16$) acquired at routine diagnostic post-mortem at the same institution. Controls had no documented history of TBI. Full clinical and demographic information, including age, sex and cause of death, is provided for all groups in Table 1.

Table 1 Demographic and clinical data for all post-mortem cases

	TBI Cases ($n = 18$)	Controls ($n = 16$)
Age		
Mean (range)	44.1 years (16–59 years)	43.0 years (16–60 years)
Median	51 years	49 years
Males	10 (55.6 %)	10 (62.5 %)
Mean survival time (range)	2.3 days (6 h–7 days)	Not applicable
Median survival time	1.5 days	Not applicable
Mean post-mortem delay	50 h (3–120 h)	43 h (4–120 h)
Assault	3 (17 %)	Not applicable—all control cases have no known history of TBI
Fall	10 (55 %)	
MVC	5 (28 %)	
Cause of death		
TBI	17 (94.4 %)	0 (0 %)
Bronchopneumonia/ARDS	1 (5.6 %)	1 (6.3 %)
Sudden unexpected death due to epilepsy	0 (0 %)	3 (18.8 %)
Acute cardiovascular death	0 (0 %)	4 (25.0 %)
Inhalation gastric contents	0 (0 %)	1 (6.3 %)
Drug overdose (paracetamol/coproxamol)	0 (0 %)	1 (6.3 %)
Acute death associated with amphetamine	0 (0 %)	1 (6.3 %)
Bronchopneumonia secondary to malignancy	0 (0 %)	2 (12.5 %)
Non-hodgkin's lymphoma	0 (0 %)	1 (6.3 %)
Septicemia	0 (0 %)	2 (12.5 %)

ARDS Acute respiratory distress syndrome, *MVC* motor vehicle collision

Human brain tissue preparation

For all examinations, the intact brain was immersed in 10 % formol saline at autopsy and fixed for at least 3 weeks prior to dissection. Sampling using a standardized protocol and paraffin embedding was performed as described previously [26]. Analyses were performed using hemi-coronal sections of the parasagittal cortex at the level of the mid-thalamus to include the cingulate gyrus and corpus callosum. This region was selected given its midline location and known susceptibility to DAI [1, 2, 34, 35, 37].

Immunohistochemical labeling of human and swine tissue

Paraffin-embedded tissue from both swine rotational injury studies and human post-mortem studies were subjected to routine histology including haematoxylin and eosin (H&E) staining as well as immunohistological techniques as described below. All tissue examinations were performed on 8 μm sections.

Single immunohistochemical labeling

Following deparaffinization and rehydration, sections were immersed in aqueous hydrogen peroxide (15 min) to quench endogenous peroxidase activity. Antigen retrieval was performed in a microwave pressure cooker with immersion in Tris EDTA buffer. Subsequent blocking was achieved using 50 μl of normal horse serum (Vector Labs, Burlingame, CA, USA) per 5 ml of Optimax buffer (BioGenex, San Ramon, CA, USA) for 30 min. Incubation with the primary antibodies was performed for 20 h at 4 °C. Specifically, Ab2233, rabbit serum reactive with the calpain-generated neoepitope at the carboxyl-end of the calpain-derived α-spectrin *N*-terminal fragment, SNTF (αII-spectrin residues 1–1176) [54, 62] was applied at 1:12 K (human) and 1:17.5 K (swine). The specificity of this cleavage site-specific antibody for SNTF generated by calpain proteolysis has been well established by Western blot, protease digest, and protease inhibitor studies [54, 61, 63, 66, 67]. As additional confirmation of the specificity of the antibody, a subset of sections from both human TBI cases and the swine model were also labeled with independent antiserum generated in different rabbits. This included Ab37 [57] and Ab2234 (which was subjected to antigen-affinity purification). A synthetic peptide corresponding to the calpain-generated neoepitope in SNTF (CAQQEVY) was conjugated covalently to maleimide-activated Sepharose via the cysteine side chain and the resulting resin used for affinity purification of SNTF-specific antibodies.

Adjacent, serial sections were labeled with an antibody reactive for the *N*-terminal amino acids 66–81 of the amyloid precursor protein (APP) (Millipore, Billerica, MA) at 1:50 K (human) or 1:80 K (swine) as the standard approach for the clinico-pathological detection of axonal pathology [22, 59]. Mouse monoclonal antibodies specific for additional neurofilament subtype markers of axonal injury were also applied to all animals and human cases including compacted neurofilament-M (RMO-14; Cell signaling technology, Danvers, MA) at 1:1 K, non-phosphorylated neurofilament-H (SMI-32 [76]; Biolegend, San Diego, CA) at 1:300 and neurofilament-68 (NF-68) (Biosensis, Thebarton, Australia) at 1:500. After rinsing, sections were incubated with the appropriate biotinylated secondary antibody for 30 min (Vector Labs, Burlingame, CA, USA), followed by an avidin biotin complex as per the manufacturer's instructions (Vectastain Universal Elite kit, Vector Labs, Burlingame, CA, USA). Finally, visualization was achieved using the DAB peroxidase substrate kit, as per manufacturer's instructions (Vector Labs, Burlingame, CA, USA). Counterstaining with haematoxylin was performed and sections were examined using light microscopy on a Nikon Eclipse 80i microscope (Nikon, Tokyo, Japan). Positive control tissue for IHC included sections containing the corpus callosum from a case of previously established DAI. Omission of the primary antibody was performed on the same material to control for non-specific binding.

Double and triple immunofluorescence labeling

Following single immunolabeling, a subset of SNTF positive human cases ($n = 6$) and all swine studies were selected for further examination by double or triple fluorescent immunolabeling with SNTF and APP, pan-neurofilament-H (NF-H), non-phosphorylated NF-H, NF-68 and compacted neurofilament-M. Specifically, following deparaffinization and rehydration of sections, antigen retrieval and blocking were performed as described above. The same anti-SNTF antibody was applied overnight (4 °C) at 1:7.5 K (swine) and 1:1 K (human). After rinsing, sections were incubated in a biotinylated donkey anti rabbit secondary antibody (Vector Labs, Burlingame, CA, USA) for 30 min followed by a streptavidin, Alexa Fluor 568 conjugate for 2 h at room temperature. Next, the following antibodies were applied serially overnight at 4 °C including mouse anti-APP antibody (Millipore, Billerica, MA) at 1:8 K, goat anti-APP [60, 85] at 1:1 K, mouse anti-pan-NF-H (Sigma, St Louis, MO) at 1:1.8 K, RMO-14 (Cell signaling technology, Danvers, MA) at 1:50, non-phosphorylated NF-H (SMI-32; Biolegend, Dan Diego, CA) at 1:50 or NF-68 (Biosensis, Thebarton, Australia) at 1:75. The corresponding Alexa Fluor donkey anti-mouse (488) or donkey anti goat (647) IgG secondary antibodies were applied for 2 h at room temperature. Serial sections of positive control tissue (human and swine) were subjected

to the entire procedure with omission of subsets of primary antibodies to control for non-specific immunofluorescence (Supplementary Fig. 1). Following rinsing, sections were coverslipped using fluorescence mounting medium (Dako, Carpinteria, CA) and visualized using a confocal Nikon Eclipse Ti microscope (Nikon, Tokyo, Japan).

Analysis of immunohistochemical findings

All observations were conducted blind to demographic and clinical information by 2 independent observers (VJ and WS). Cases were reviewed independently and inter-rater reliability was >90 %. Those slides where there was disagreement were reviewed by both observers until consensus was reached.

Quantitative analyses of swine tissue were performed blind to the injury status. Specifically, for all animals, triple-labeled sections for both SNTF + APP + RMO-14 and SNTF + APP + NF-68 were subjected to high-resolution confocal imaging of approximately a 1 mm square region in the subcallosal fasciculus adjacent to the left lateral ventricle (a region with established biomechanical vulnerability). The entire 8 μm depth of the tissue was imaged and maximal-projection images acquired. The number of axonal profiles was quantified per unit area (μm) for each marker. The co-localization or absence of co-localization of markers was also quantified. An axonal profile was defined as a swollen axonal bulb or individual morphologically injured or varicose axonal profile.

Additionally, in the more heterogeneous human TBI cases, the extent of axonal pathology as revealed by both SNTF and APP staining was classified using standard semi-quantitative assessments as: 0 = absent, 1 = minimal 2 = moderate or 3 = extensive pathology. This scoring was representative of the entire hemi-coronal section of the parasagittal cortex at the level of the mid-thalamus to include the cingulate gyrus and corpus callosum.

Statistical analyses

Statistical analyses were performed using GraphPad Prism statistical software (GraphPad Software Inc. La Jolla, CA). The Fisher's exact test was used to assess differences in the presence of axonal pathology between human TBI cases versus controls.

Results

Clinical presentation following mTBI in swine

After being returned to housing (within 30 min of injury), all animals regained consciousness and mobilized rapidly (within 5–10 min) following withdrawal of isoflurane, indicating that there was no prolonged loss of consciousness. Following recovery from anesthesia, all animals were fully conscious and alert. Mental status was unaltered and all animals resumed normal feeding and drinking behavior within 1–2 h. Consistent with the clinical presentation of mild TBI, all animals had a normal neurological examination and did not display any focal neurological deficits. Specifically, the animals displayed normal posture, tone, gait, power, sensation and proprioception. Examination of cranial nerves was normal.

Gross neuropathological examination and H&E staining following mTBI in swine

Following rotational injury, the brains of all animals were normal on gross pathological examination and indistinguishable from sham animals. Consistent with mild TBI clinically, there was no evidence of any focal lesions, including hemorrhagic lesions. In addition, the hemispheres were symmetrical with no evidence of brain swelling or raised intracranial pressure (ICP). Consistent with these observations, H&E staining demonstrated an absence of any hemorrhagic or ischemic lesions, or neuronal pyknosis in any animals.

Axonal pathology (APP IHC) following mTBI in swine

Examination using IHC specific for APP revealed swollen and morphologically altered axons consistent with transport interruption secondary to axonal cytoskeletal damage and indistinguishable from those observed in human DAI [1–3, 22, 23, 34, 35, 59] (Fig. 1). Specifically, many axonal APP-positive profiles had the appearance of large spheroids and, while dependent on the plane of view, likely represent disconnected axon terminals. In contrast, other APP reactive axons displayed a more fusiform or varicose morphology, often with multiple swellings along the axon length and greatly increased in diameter (Fig. 1b–d, f, g). Much more rarely, axons with limited APP accumulation and an undulating morphology were observed, although predominant only at the most acute survival time point (6 h post-injury).

Mapping of APP-immunoreactive axons with an abnormal morphology revealed these to be consistently observed in a stereotypical, multifocal distribution affecting the subcortical and periventricular white matter and midline structures of all injured animals (Fig. 1a). Notably, the pattern and distribution of pathology was not symmetrical, with the left hemisphere (the leading hemisphere during coronal rotation) displaying an increased density of pathology in the deep white matter and with extensive pathology in the periventricular white matter of the lateral ventricles.

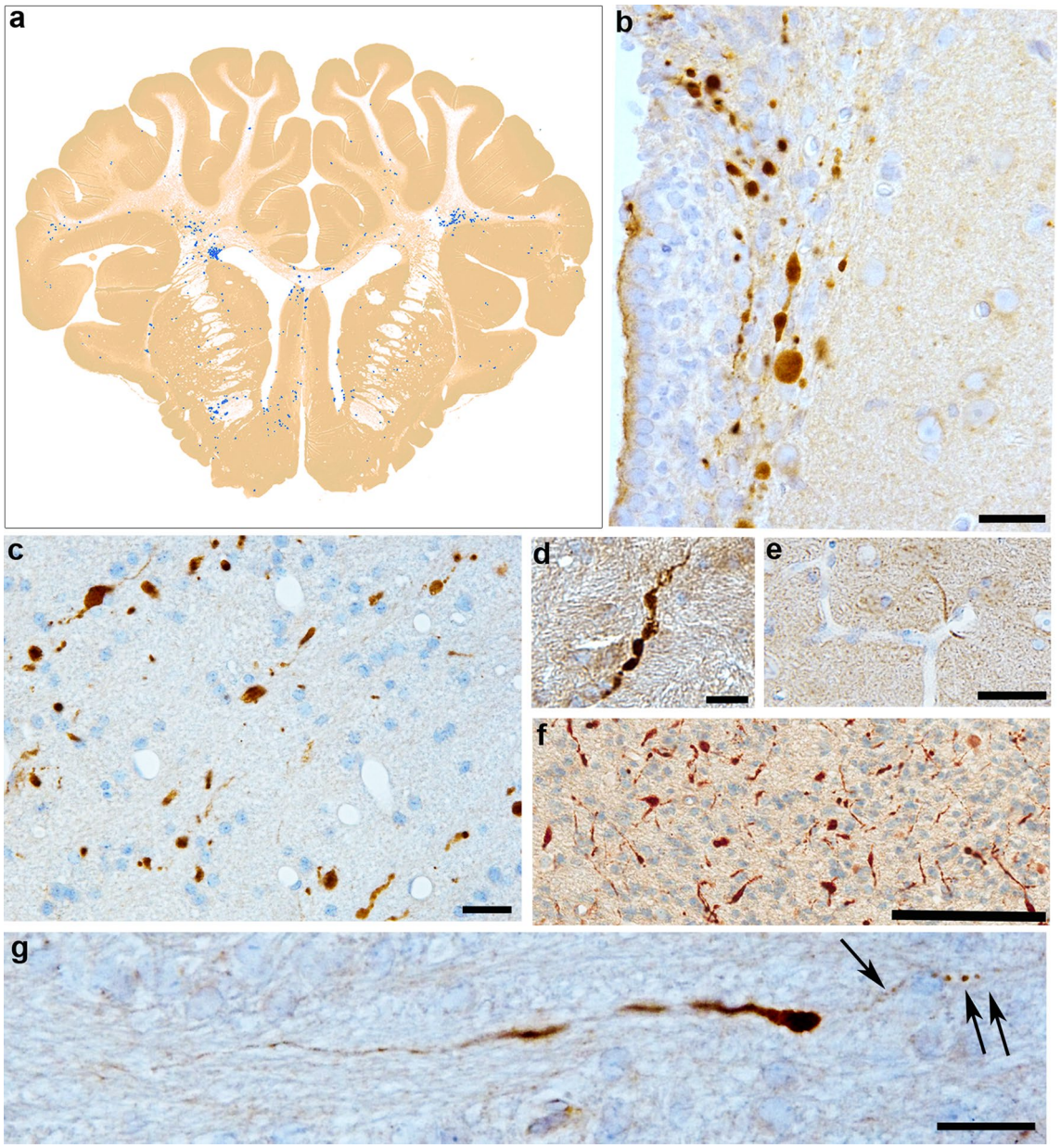

Fig. 1 APP (antibody 22C11) accumulation in injured axons following rotational acceleration–deceleration injury in swine. **a** Whole brain coronal map of APP accumulating axonal pathology 48 h following injury. **b** Extensive APP-positive axonal bulbs and swellings in the periventricular white matter 6 h following injury. Note the associated disruption of the ependymal cell layer. **c** APP accumulating axons 48 h following injury displaying a variety of injured morphologies including terminal swellings, beading and intact fusiform profiles with multiple points of transport interruption. **d** A highly fusiform APP-positive axon 48 h post-injury indicating multiple points of cytoskeletal damage and transport interruption. **e** A single APP-positive degenerating axon underlying a vessel at 48 h post-injury, a common site of axonal pathology likely reflecting the impingement of axons on the comparatively more rigid vessel during dynamic motion. **f** Extensive APP-positive axonal pathology in the periventricular white matter 72 h following injury. **g** A single APP-positive injured axon 6 h post-injury with APP accumulating along its length and giving a fusiform appearance. Note the largest point of swelling is followed by a section of the axon with a much narrower diameter and beaded appearance likely indicative of complete transport interruption with distal Wallerian-like degeneration (*arrows*). *Scale bars* (**b**–**e**, **g**) 25 µm, **f** 100 µm

In contrast, the right (non-leading) hemisphere displayed more frequent axonal pathology in the rostral digitate white matter (Fig. 1a). This hemisphere-dependent distribution of pathology was conserved between animals and consistent with a direct mechanical etiology. Moreover, injured axons were frequently observed underlying or around vessels which, as comparatively rigid structures, can injure axons during dynamic brain deformation (Fig. 1e).

Consistent with previous examinations in both animal models and clinical DAI [23, 34, 35, 59], axonal pathology was observed at all time points post-injury from 6 to 72 h. Notably, while the distribution was the same at 6 h post-injury, the extent of pathology was not as marked when compared to that following 48–72 h survival. As all animals were injured with the same input parameters, resulting in a narrow range of peak rotational velocities for each study, the resultant neuropathological outcome was highly consistent between animals. Maps of pathology indicated virtually identical pattern and distribution of APP pathology between all animals at each time point. The extent of pathology was also highly consistent between all animals within a given survival time point as per quantitative analyses (Fig. 4). Notably, of the 2 animals examined at 48 h, one animal had a slightly higher rotational level that likely accounts for the increased standard deviation in this group. No axonal pathology was observed in any sham animals using APP IHC.

SNTF immunoreactivity following mTBI in swine

Following rotational acceleration injury, SNTF positive structures with the morphological appearance of injured axons were found in the white matter in a pattern and distribution consistent with a biomechanical etiology. The specificity of the axonal immunoreactivity for SNTF was confirmed in a subset of serial sections using an additional independent antiserum, Ab37, and the antigen-affinity purified SNTF antibody Ab2234. All 3 antibodies revealed highly consistent patterns of immunoreactivity for axonal profiles with altered morphologies (undulations, swellings, degeneration) in the injured animals (Supplementary Fig. 2).

Interestingly, SNTF positive axons were frequently of a much smaller diameter than typically observed with APP IHC. At 6 h post-injury, SNTF immunoreactivity was frequently observed in a confluent or patchy distribution along axons that appeared intact and without notable varicosities or swellings (Fig. 2b–e). However, several axons displayed an undulating morphology (Fig. 2e). In contrast, by 48 and 72 h post-injury, virtually all SNTF positive axons displayed a more pathological phenotype with occasional small swellings and beading, indicative of a rapid degenerative process (Fig. 2f, g, i, k). Double labeling with a pan-NF-H antibody (which identifies all NF-H regardless of phosphorylation state) confirmed the SNTF positive structures were axons (Fig. 3j–o). Notably, there was no SNTF immunoreactivity in neuronal cell bodies or dendrites at any time point examined (Supplementary Fig. 2). No axonal pathology was observed in any sham animals using SNTF IHC (Fig. 2a, h).

Comparison of APP and SNTF immunoreactivity following mTBI in swine

Double labeling IHC was performed specific to both SNTF and APP to evaluate for their potential co-localization. Interestingly, in large part, APP and SNTF appeared to identify different axonal populations. Specifically, while occasional co-localization between APP and SNTF was present in damaged axons, frequent APP-positive/SNTF-negative axons were observed (Fig. 3a–f). In addition, SNTF positive/APP negative axons were also identified (Fig. 3a–c, g–i). Notably, this was observed at all time points examined from 6 to 72 h post-injury indicating that SNTF identifies an axonal population distinct from APP-positive axons in the traumatically injured brain. Overall, the number of SNTF positive axonal profiles was less than that observed using APP IHC at all time points post-injury with a smaller number of axonal bulbs and varicose profiles (Fig. 4). Specifically, of the total number of axonal profiles per unit area detected by APP and SNTF at 6 h post-injury, 44 % were detected by SNTF only, 51 % by APP only and 5 % by both SNTF and APP. At 48 h survival, 19 % were detected by SNTF only, 79 % by APP only and 2 % by both SNTF and APP. This remained similar at 72 h where 24 % were detected by SNTF only, 75 % by APP only and 1 % by both SNTF and APP.

Comparison of SNTF with APP and neurofilament subtypes as markers of axonal pathology following mTBI in swine

Previous work in both animal models and humans has demonstrated that immunohistochemistry specific for various neurofilament subtypes can identify axonal pathology with varying degrees of success. Given the above observation that SNTF positive axons can exist in the absence of APP accumulation, we next sought to determine whether neurofilament IHC identifies yet another distinct population of axons or if there was overlap of neurofilament subtype markers with APP or SNTF. As such, we performed series of triple labeling studies with SNTF, APP and each of three previously identified markers including non-phosphorylated NF-H (SMI-32) [24, 56, 83], NF-68 [15, 24, 48, 83] and NF-M (RMO-14) [9–11, 13, 51, 77] to explore the relative role of these markers in identifying damaged axons.

Non-phosphorylated NF-H (SMI-32)

Consistent with previous work [24, 83], swine demonstrated normal immunoreactivity for non-phosphorylated NF-H in subgroups of neurons, including staining of the cell body, dendrites and axons. This was consistent

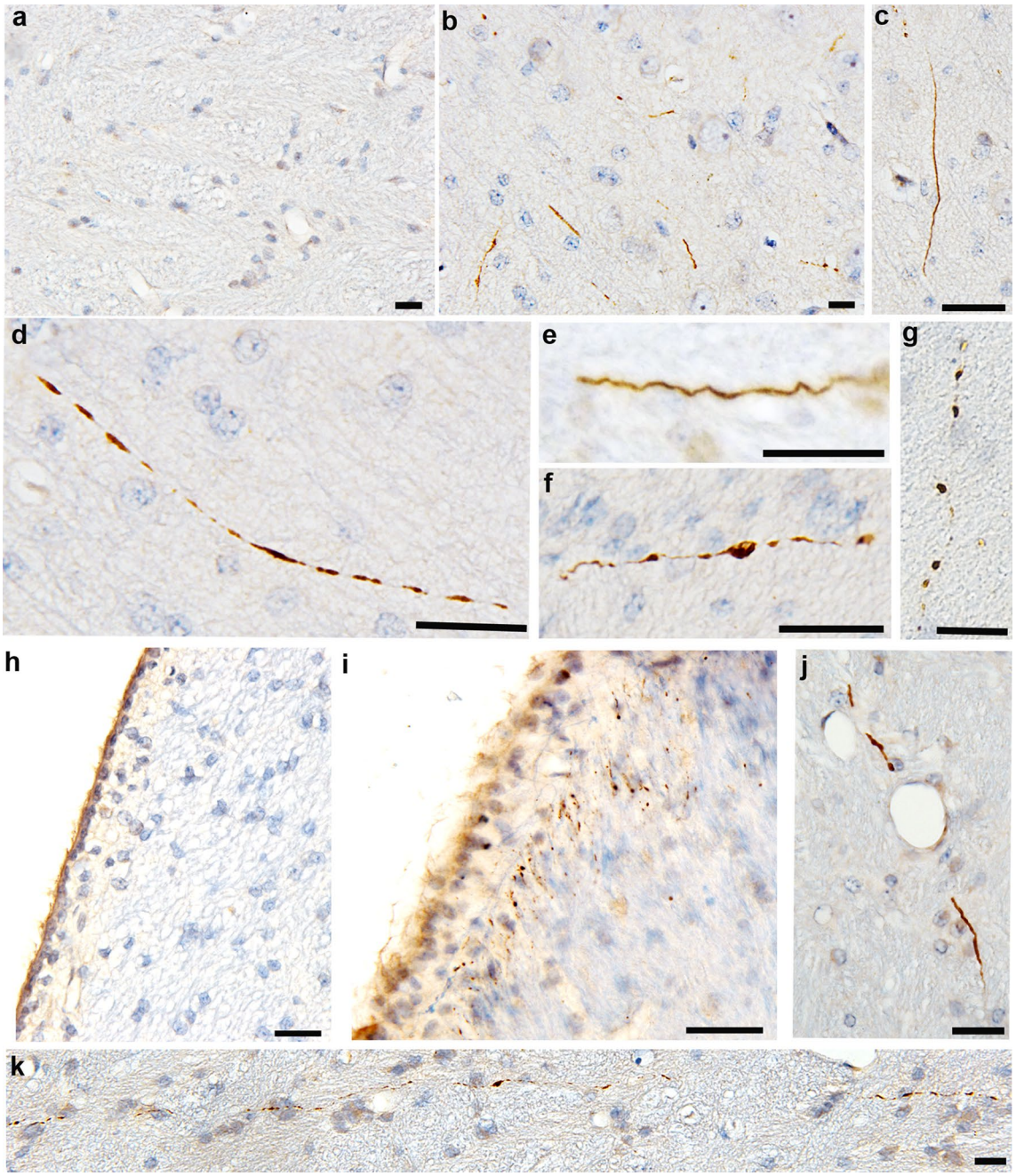

Fig. 2 IHC specific for SNTF (Ab2233) showing the range of axonal pathologies following mTBI in swine. **a** An absence of SNTF immunoreactivity in the subcortical white matter of a sham animal. **b** Multiple SNTF positive profiles in the subcortical white matter of the left hemisphere 6 h post-injury. Note that the axons are of comparatively smaller diameter to those reactive for APP with limited evidence of extensive swelling. **c** A single axon reactive for SNTF 6 h post-injury in the periventricular region which remains intact along the immunoreactive portion without overt swellings. **d** A single axon reactive for SNTF 6 h post-injury in the subcortical white matter with a more patchy immunoreactivity extending approximately 100 µm. **e** A single SNTF positive axon 6 h post-injury in the left subcortical white matter showing an undulating morphology indicative of cytoskeletal damage with an absence of large swellings. **f** 48 h post-injury, a single SNTF positive axon with some small swellings and a more degenerative morphology. **g** A single SNTF positive axon at 72 h post-injury in the subcortical white matter showing a highly beaded and degenerative morphology. **h** An absence of SNTF positive profiles in the periventricular region of a sham animal. **i** The same region as **h** showing multiple small accumulations of SNTF 48 h post-injury. **j** An axon positive for SNTF close to a vessel, a known site of mechanical vulnerability. **k** What appears to be a single SNTF positive axon with multiple foci of SNTF immunoreactivity extending for several hundred microns through the subcortical white matter 72 h post-injury in a region of known mechanical vulnerability. All *scale bars* 25 µm

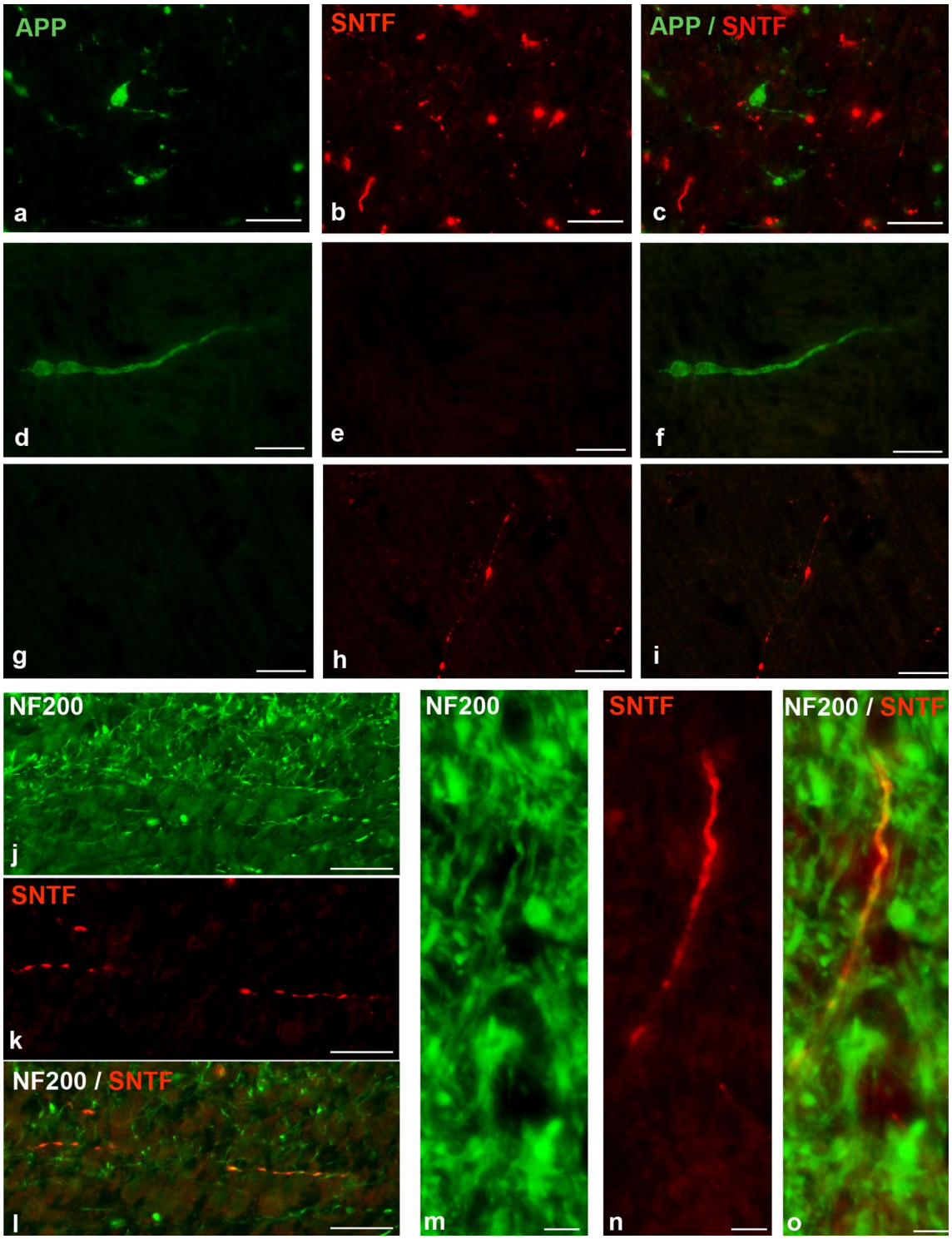

Fig. 3 Double label IHC following rapid rotational acceleration/deceleration in swine using APP (22C11) and SNTF (Ab2233). **a–c** A region of the subcortical white matter showing APP and SNTF reactive profiles with notably little overlap at 72 h post-injury. **d-f** An APP-immunoreactive axonal swelling that is SNTF negative and **g-i** an SNTF immunoreactive axonal profile that is APP negative at 48 h post-injury. Note the reduced diameter of the SNTF positive axon when compared to that of the APP-immunoreactive axon. SNTF reactive profiles were also immunoreactive for pan-NF-H (sigma) confirming that SNTF reactive profiles are axons (**j–l**, **m–o**). All *scale bars* 25 μm

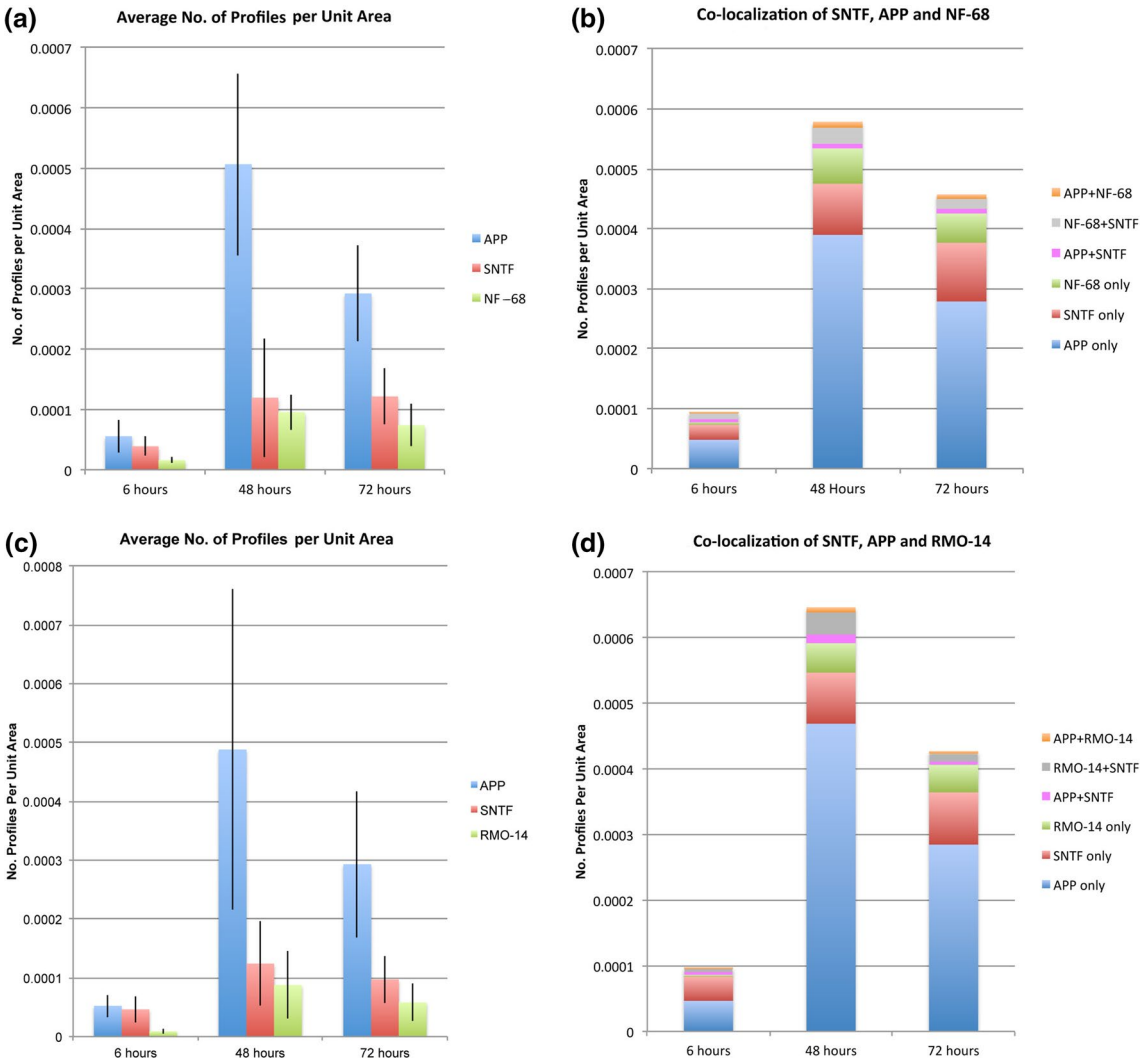

Fig. 4 Graphs demonstrating the average number of profiles per unit area (μm) following mTBI in swine for **a** SNTF, APP and NF-68 and **c** SNTF, APP and RMO-14. In addition, *graphs* **b** and **d** demonstrate the relative co-localization or absence of co-localization of each marker in identifying pathology at 6, 48 and 72 h post-mTBI identified using triple labeling for SNTF, APP and NF-68 and SNTF, APP and RMO-14, respectively

between both sham and injured animals. However, upon examination of tissue following mTBI in swine, SMI-32 did not readily identify axons with an altered morphology, even in regions with dense pathology as revealed by APP staining on serial sections. This finding was independent of antibody concentration (data not shown). Notably, this is consistent with previous work demonstrating that identification of axonal pathology in swine using SMI-32 is relatively unsuccessful versus that described in rodent models [56, 69].

As observed in single labeled sections in swine, triple immunofluorescent labeling performed with SMI-32, SNTF and APP demonstrated independent populations of SNTF- and APP-positive injured axons. While some co-localization could be observed with SNTF in non-swollen, SMI-32 positive axons, there were no swollen or morphologically altered SMI-32 positive axons that were clearly distinguishable from those observed in shams (Fig. 5a–d). Interestingly, in some cases, SMI-32 positive axons with a normal morphology were observed feeding into a terminal bulb that was densely APP positive, yet with a clear absence of SMI-32 accumulation in the terminal bulb itself (Fig. 5a, b).

NF-68

NF-68 immunoreactivity was present in axons and occasional dendrites with a normal morphology in both sham and injured animals (Fig. 5e). However, following injury,

in addition to axons with a normal appearance, single labeling with NF-68 revealed occasional large swollen axonal profiles consistent with the appearance of terminal axonal bulbs as has been previously described in swine and other models, as well as humans [15, 24, 48, 83] (Fig. 5f). These were observed in regions consistent with biomechanical injury. Notably, baseline axonal staining in normal axons limited visualization of more subtle swellings or accumulations. Subsequent triple labeling studies with SNTF, APP and NF-68 demonstrated that NF-68 positive bulbs could occasionally be observed overlapping in terminal bulbs with both SNTF and APP (Fig. 5i). However, at all time points, all 3 markers identified injured axons in the absence of either of the other markers, identifying 3 novel populations of pathological axons at any given time (Fig. 5h, i). Notably, while NF-68 and APP identified larger swollen profiles, axons that were positive for SNTF only were typically of smaller diameter and/or beaded as described above. Although NF-68 positive bulbs could be observed at 6 h post-TBI, they were notably more numerous by 48–72 h post-TBI (Fig. 5h, i). Quantification of the number of axonal profiles revealed that of the total number of axonal profiles per unit area detected by triple labeling using APP, SNTF and NF-68, 17 % were detected by NF-68 at 6 h. Of these, 5 % were detected by NF-68 alone, 10 % co-localized with SNTF and 2 % co-localized with APP. At 48 h, 17 % were also detected by NF-68. Of these, 10 % were detected by NF-68 alone, 5 % co-localized with SNTF and 2 % co-localized with APP. This remained similar at 72 h where 16 % of axonal profiles were detected by NF-68. Of these, 10 % were detected by NF-68 alone, 4 % co-localized with SNTF and 2 % co-localized with APP (Fig. 4).

Compacted neurofilament-M (RMO-14)

Immunoreactivity for RMO-14 was present in subgroups of neurons and axons with a normal morphology, consistent between sham and injured animals (Fig. 5j–n). Following mTBI, labeling for RMO-14 identified swollen axonal bulbs in regions consistent with biomechanical injury at all time points (Fig. 5k, l, n). However, as with NF-68, the extent of pathology identified was minimal when compared to that identified using APP.

Nonetheless, triple labeling with SNTF, APP and RMO-14 again demonstrated some minimal overlap with APP and SNTF positive populations of injured axons, virtually always in terminal bulbs. Again, all 3 markers identified axons with an altered morphology in the absence of co-localization with either of the other markers (Fig. 5n).

For all triple labeling studies shown in Fig. 5, images of the merged and individual channels (red, green and purple) are shown in Supplementary Fig. 4.

Of the total number of axonal profiles per unit area detected by triple labeling using APP, SNTF and RMO-14, 9 % were detected by RMO-14 at 6 h. Of these, 3 % were detected by RMO-14 alone, 5 % co-localized with SNTF and 1 % co-localized with APP. At 48 h 13 % were also detected by RMO-14. Of these, 7 % were detected by RMO-14 alone, 5 % co-localized with SNTF and 1 % co-localized with APP. This remained similar at 72 h where 14 % of axonal profiles were detected by RMO-14. Of these, 10 % were detected by RMO-14 alone, 3 % co-localized with SNTF and 1 % co-localized with APP (Fig. 4).

Axonal pathology identified by APP IHC following TBI in humans

APP IHC revealed axonal pathology in 17 of 18 (94 %) of TBI cases versus 3 of 16 (19 %) controls ($p \leq 0.0001$). APP immunoreactivity was observed from 6 h to 7 days post-TBI in the form of classic terminal axonal bulbs and swollen fusiform profiles as has been previously described in detail [22, 34, 35, 59] (Fig. 6a). As expected, a range of patterns and distributions of pathology were observed. This included APP-positive axons in a pattern and distribution consistent with traumatic diffuse axonal injury, with axonal profiles observed individually scattered or in small clusters, often in a single directional plane. In contrast, other cases displayed superimposed, widespread waves of axonal APP immunoreactivity in keeping with axonal pathology as a result of the vascular complications of raised intracranial pressure [19, 20, 27, 29, 34, 53].

Of the TBI cases, 2 of 18 (11 %) displayed minimal axonal pathology identified using APP, with few scattered or isolated foci of pathological regions (score 1). 6 of 18 cases (33 %) had moderate axonal pathology with multiple foci of APP-positive axons in both dense regions associated with lesions or diffusely scattered axons (score 2) and the final 9 of 18 cases (50 %) displayed extensive APP axonal pathology (score 3) with numerous foci of pathology and widespread and diffuse pathology occupying all regions of white matter examined (Fig. 6c). This compared to controls where just 1 case (6 %) displayed moderate APP immunoreactivity (score 2) and 2 cases (12.5 %) displayed minimal pathology (score 1). Notably, these controls displayed axonal pathology in a pattern and distribution in keeping with hypoxic/ischemic injury, likely indicative of an agonal event near the time of death [19, 20, 27, 29, 34, 53].

SNTF immunoreactivity following TBI in humans

SNTF immunoreactive axonal profiles with a morphological appearance consistent with injured and degenerating axons

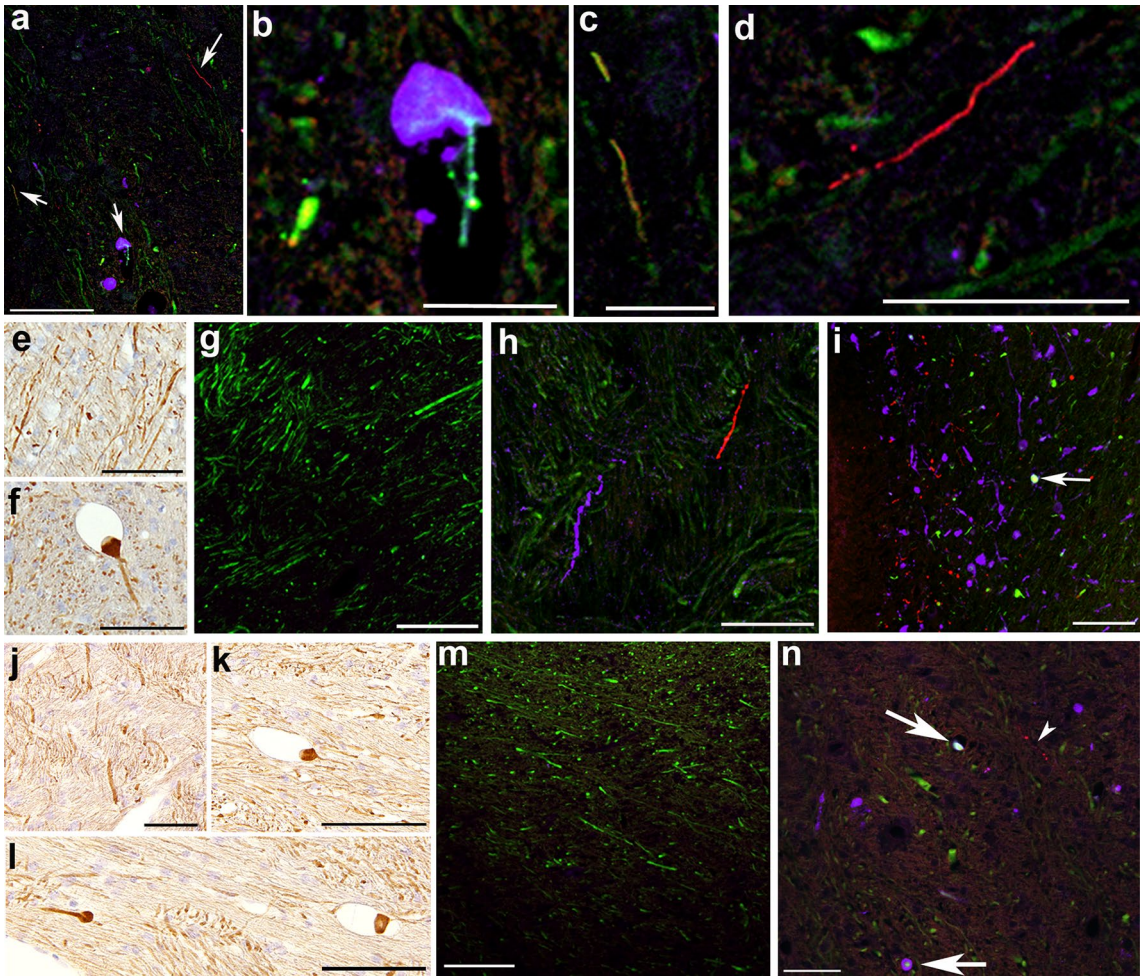

Fig. 5 A representative example of triple immunofluorescent labeling 48 h following mTBI in swine showing SNTF (2233) (*red*), SMI-32 (*green*) and APP (*purple*) (**a**–**d**). Regions of interest from (**a**) identified with *arrows* are shown at high magnification (**b**–**d**). Note that while there is co-localization between SNTF and SMI-32 in some axons, they appeared to have a normal morphology without notable swelling. In addition, APP-positive swellings did not co-localize with SMI-32 (**b**). Notably, many SNTF axons did not co-localize with either SMI-32 or APP (**d**). NF-68 immunoreactivity in a sham animal (**e**) and following mTBI in swine (**f**). Note the clear baseline staining in normal axons in shams (**e**). In contrast, large swollen axonal bulbs could be seen post-mTBI (**f**, **i**). Representative examples of triple immunofluorescent labeling in swine with SNTF (2233) (*red*), NF-68 (*green*) and APP (*purple*) (**g**–**i**). Sham animals displayed an absence of APP or SNTF immunoreactivity, but clear baseline NF-68 in axons was visible (**g**). At 6 h post-mTBI there are very few NF-68 positive swellings, although APP and SNTF accumulating profiles can be observed without co-localization (**h**). In contrast, by 48 h, clear NF-68 positive swellings can be observed (**i**), few of which co-localized with APP and or SNTF (**i**, *arrow*). RMO-14 staining in sham animal (**j**) and 48 h following mTBI in swine (**k**–**l**). Note the clear baseline staining in shams (**j**). In contrast, large swollen axonal bulbs could be seen post-mTBI (**k**–**l**). Representative example of triple immunofluorescent labeling in swine with SNTF (2233) (*red*), RMO-14 (*green*) and APP (*purple*) (**m**–**n**). Sham animals displayed an absence of APP or SNTF immunoreactivity, yet baseline RMO-14 immunoreactivity in axons was observed (**m**). At 48 h post-mTBI, RMO-14 positive swellings can be observed, with (*arrows*) and without co-localization with APP and SNTF (**n**). However, many injured axons displayed an absence of co-localization between any markers. Note the more subtle beaded profiles positive for SNTF alone (**n**, *arrowhead*). *Scale bars* **a**, **e**–**g**, **j**–**m** 100 μm, **b** 25 μm, **c** 12.5 μm, **d**, **h**, **i** 50 μm

were observed in 17 of 18 (94 %) TBI cases versus just 2 of 16 (12.5 %) controls ($p \leq 0.0001$). SNTF immunoreactive axons with an abnormal morphology were identified in cases across the survival range from 6 h to 7 days post-injury and corresponded to the cases that had APP-positive injured axons. Notably, SNTF axons displaying the classical appearance of swollen, fusiform axons and terminal axonal bulbs were observed and similar to those described using APP IHC (Fig. 6b, e–h). In addition, several early acute cases displayed axons with an undulating morphology (Fig. 6e). Notably, fewer smaller diameter axons were observed when compared with the swine model of mild TBI.

Using the maps of pathology generated, the pattern and distribution of pathology identified using SNTF IHC was

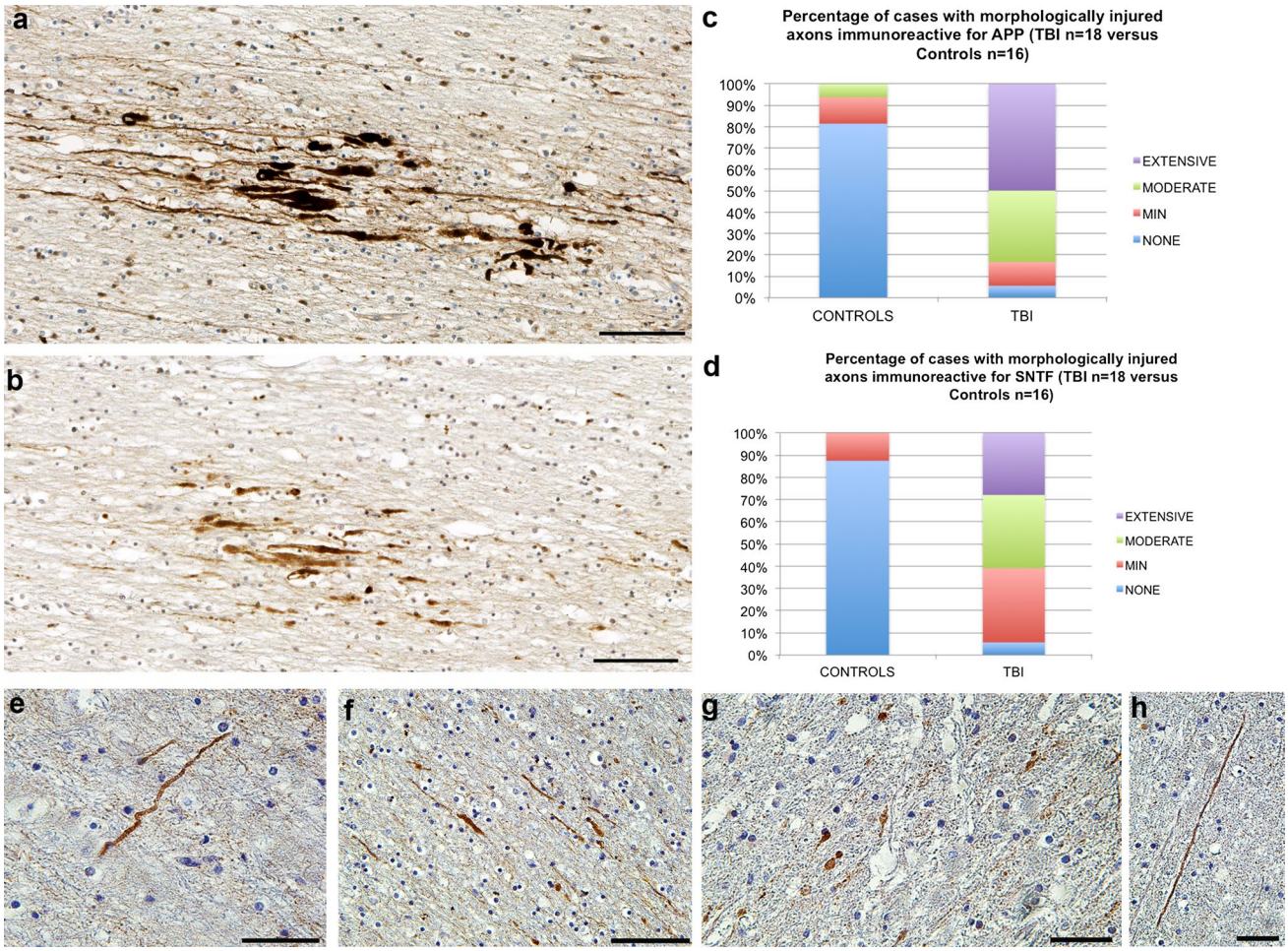

Fig. 6 SNTF (Ab2233) versus APP (22C11) immunoreactivity acutely following severe TBI in humans. APP (**a**) and SNTF (**b**) immunoreactive profiles including fusiform swellings and terminal axonal bulbs in serial sections of the white matter adjacent to the cingulate gyrus in an 18 year old male who died 10 h following severe TBI. Note the more extensive pathology revealed by APP IHC. *Graphs* showing semi-quantitative scores for the percentage of cases with APP (**c**) and SNTF (**d**) immunoreactive axonal profiles. The range of SNTF (Ab2233) immunoreactive profiles in white matter following acute severe TBI in humans shown in **e** SNTF immunoreactive axon with an undulating morphology in the parasagittal white matter of a 59 year old male, 4 days following a TBI caused by a fall. **f** Swollen and fusiform SNTF immunoreactive profiles in the corpus callosum of an 18 year old male who died 10 h following TBI caused by an assault. **g** SNTF immunoreactive axonal bulbs and **h** a linear SNTF positive, swollen axonal profile observed in the corpus callosum of a 17 year old male who died 2 weeks following a road traffic accident. *Scale bars* **a**–**b**, **f** 100 µm, **e**, **g**–**h** 50 µm

very similar to the distribution of APP-immunoreactive axonal pathology with respect to both region and pattern. Of the TBI cases, 6 cases (33 %) displayed minimal SNTF axonal pathology (score 1), 6 cases (33 %) had moderate axonal pathology (score 2) and the final 5 cases (28 %) displayed more extensive axonal pathology (score 3) (Fig. 6d). Thus, the overall extent of axonal pathology as determined by APP IHC was greater than that identified with SNTF, of which a representative example is provided in Fig. 6a–b. However, SNTF positive axons were considerably more abundant in the human severe TBI cases when compared to the swine model of mTBI. Interestingly, consistent with previous observations of SNTF in more severe models of TBI [57], occasional neuronal somato-dendritic immunoreactivity for SNTF could be observed following severe TBI in humans (Supplementary Fig. 3). However, this was not quantified.

Of the control group, just 2 of 16 (12.5 %) cases displayed only minimal (score 1) SNTF immunoreactivity. Both of these cases also displayed APP accumulating axons and, similarly, SNTF was observed in the same regions as APP in a pattern and distribution in keeping with hypoxic/ischemic injury [19, 20, 27, 29, 34, 53]. Only one control was minimally APP positive yet displayed no SNTF reactivity. The cause of death in this case was acute paracetamol overdose.

There was no significant difference in the PM delay between TBI cases (mean 50 h; range 3–120 h) versus

controls (mean 43 h; range 4–120 h) (TTEST: $p = 0.5$). Moreover, in TBI cases, although numbers were small, there was no difference in the PM delay between those cases with absent or minimal immunoreactivity (score 0–1) versus those with moderate to extensive immunoreactivity (score 2–3) (TTEST: $p = 0.1$).

Comparison of APP and SNTF immunoreactivity following TBI in humans

As described above, fluorescent double labeling revealed both SNTF and APP-positive axons with abnormal morphologies including swollen, fusiform axons (varicosities) and terminal axonal bulbs (Fig. 7). Once again, there was not complete overlap between the axonal populations reactive for APP and SNTF. Reflective of the overall greater extent of APP immunoreactivity described above, frequent morphologically abnormal APP-immunoreactive axonal profiles were observed that had no demonstrable SNTF immunoreactivity. In addition, various other damaged axons displayed either complete or patchy co-localization of SNTF and APP. Rarely, damaged axons immunoreactive for SNTF only were observed (Figs. 7, 8).

Comparison of SNTF with APP and neurofilament subtypes as markers of axonal pathology following TBI in humans

Non-phosphorylated NF-H (SMI-32)

Human tissue demonstrated normal immunoreactivity for SMI-32 in select subgroups of neurons, including both the cell body and axons, consistent between TBI cases and controls as previously described in humans [14, 24] (Fig. 8a, d). However, following TBI, SMI-32 immunohistochemistry revealed occasional abnormal profiles including minimal undulations and occasional granular accumulations in terminal bulbs in regions where APP-positive axonal pathology was observed on serial sections (Fig. 8b, c). Nonetheless, the extent of readily identifiable

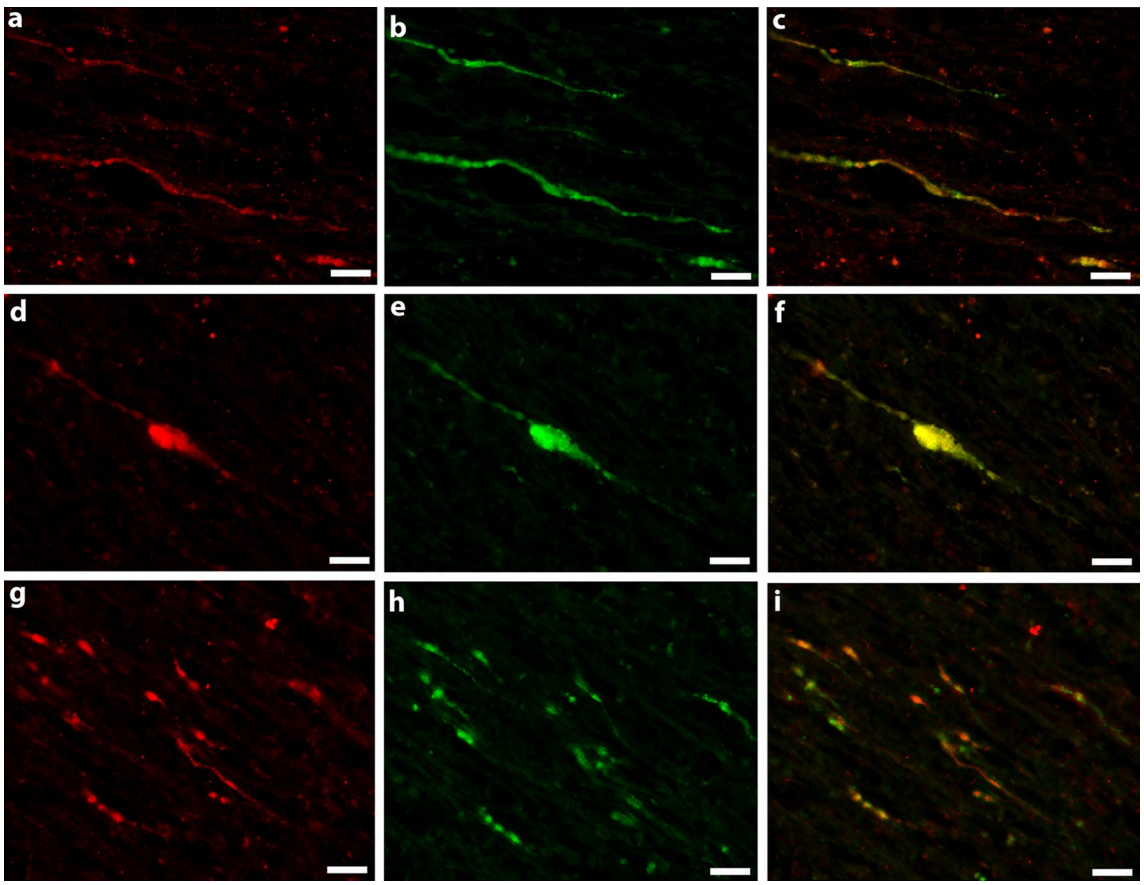

Fig. 7 SNTF (Ab2233) and APP (22C11) double labeling acutely following severe TBI in humans where SNTF is *red* and APP is *green*. (**a–c**) Shows patchy variation in the extent of APP and SNTF immunoreactivity along the length of a fusiform axon. **d–f** Shows almost complete overlap in SNTF and APP immunoreactivity in a large axonal swelling which remains connected. **g–i** Shows axons that are both reactive for either APP or SNTF only, in addition to those with co-localization. All *scale bars* 25 μm

pathology was very minimal when compared to either SNTF or APP, in part exacerbated by the high degree of baseline SMI-32 immunoreactivity in neuronal somata, dendrites and axons, limiting appreciation of more subtle swellings.

Subsequent triple labeling studies with SMI-32, SNTF and APP demonstrated some overlap between limited SMI-32 positive swellings and either SNTF or APP. Notably, SNTF immunoreactivity was observed in isolated axons or components of axons, but also frequently co-localized with large APP-positive swellings in the absence of SMI-32. While the pattern of overlapping markers was complex, only very occasional profiles could be observed with SMI-32 immunoreactivity alone (Fig. 8e).

NF-68

As above, human tissue demonstrated immunoreactivity for NF-68 in subgroups of axons with a normal morphology consistent between both TBI cases and controls (Fig. 8f–j). However, virtually no immunoreactivity could be detected in neuronal cell bodies, consistent with findings in swine and previous reports [24].

Following TBI, NF-68 revealed abnormal axonal profiles, although this was comparatively less than that identified using APP or indeed SNTF and was typically only observed in regions with extensive damage (Fig. 8g–h). This finding was supported by triple labeling studies with NF-68, SNTF and APP, which demonstrated minimal overlap between SNTF or APP in both axonal swellings and varicose profiles. However, again very occasional NF-68 swellings could be observed in the absence of APP or SNTF (Fig. 8j).

Compacted neurofilament-M (RMO-14)

RMO-14 staining identified a subset of neurons, dendrites and axons with a normal morphology consistent between TBI cases and controls (Fig. 8k–q). Following TBI, in regions of axonal pathology, RMO-14 typically identified swollen axonal bulbs or axons with an altered morphology, although again less than what was typically observed with APP (Fig. 8l, m, o–q). Nonetheless, the triple labeling with RMO-14, SNTF and APP was compelling, demonstrating that SNTF and RMO-14 frequently co-localized to individual axonal bulbs. Interestingly, SNTF and RMO-14 appeared to occupy distinct compartments within these bulbs (Fig. 8p). Notably, RMO-14 very rarely co-localized with APP. In addition to this complex co-labeling, all 3 markers demonstrated injured axonal profiles, or components of varicose axons, positive for each individual marker alone (Fig. 8o–q). This indicates that all 3 markers can identify different populations or components of injured axons post-TBI.

For all triple labeling studies shown in Fig. 8, images of the merged and individual channels (red, green and purple) are shown in Supplementary Figs. 5 and 6.

Discussion

Here we demonstrate that immunostaining for the calpain cleaved *N*-terminal fragment of alpha-II spectrin, SNTF, may reveal a unique and previously unidentified subpopulation of injured axons following TBI. In the absence of tissue from humans following mTBI, we examined a swine model of mTBI, where SNTF was found acutely in axons without large swellings, which were frequently distinct from injured axons immunoreactive for APP or neurofilament subtypes. Following severe TBI in humans, while there was overlap between the localization of SNTF and APP in swollen axon profiles, a small subset of SNTF positive axons displayed no APP accumulation. Moreover, while there was clear co-localization between SNTF and compacted neurofilaments in damaged axons, other SNTF positive axons had no overlap. Interestingly, neurofilament subtypes were also observed to exist in injured axons without either APP or SNTF. This evidence suggests that there might be multiple distinct phenotypes of axonal pathology post-TBI. SNTF positive axons may represent a unique phenotype of axonal injury, where degeneration is primarily due to proteolysis rather than following transport interruption. In addition, the identification of rapid and axon-specific accumulation of SNTF after TBI is consistent with the reported association of blood SNTF elevations and white matter abnormalities detectable with diffusion tensor imaging [62] and supports the potential diagnosis of DAI in individuals found to have elevated serum SNTF levels after mild TBI [62, 65]. Together these data may provide a novel approach to perform more comprehensive neuropathological analyses of DAI.

The spectrin tetramer is an actin-binding component of the submembranous cortical axonal skeleton important for normal development. In addition to playing a critical structural role, spectrin proteins have a complex physiological role in membrane function [4]. SNTF is a stable *N*-terminal 1176 residue fragment of the spectrin α-subunit generated via cleavage of alpha-II spectrin by calcium-dependent calpain proteases [54, 64]. In TBI, spectrin breakdown products have commonly been observed in multiple animal models [13, 42, 56, 57], suggesting that calcium influx is an important initial mediator of post-traumatic proteolysis. Indeed, massive calcium influx has been demonstrated to occur via both mechanically mediated ion channel dysfunction and alterations to membrane permeability [12, 33, 48,

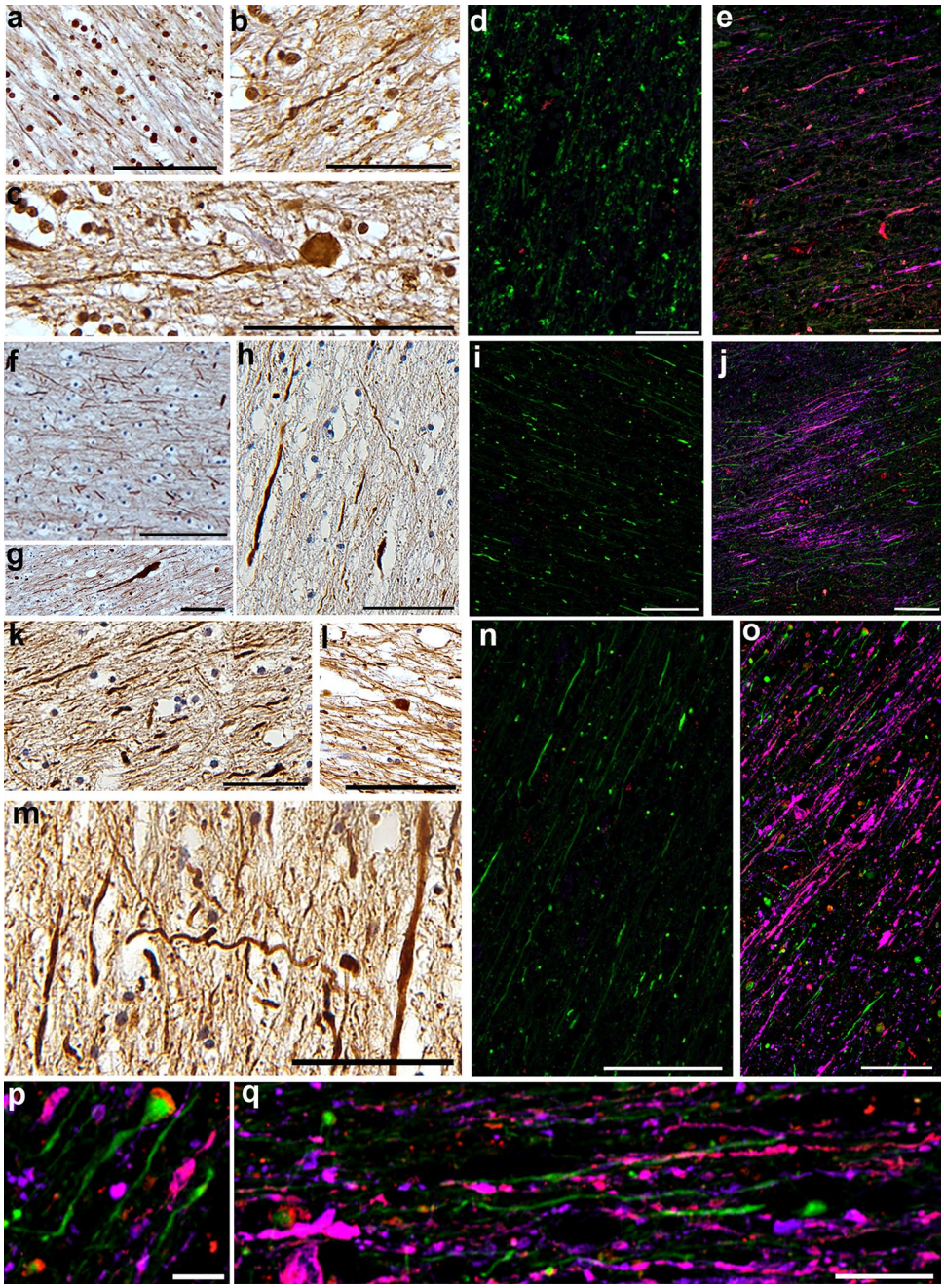

49, 82]. In particular, an in vitro model of axonal injury directly demonstrated that calcium influx occurs with dynamic stretching of axons and leads to calpain activation, spectrin proteolysis and SNTF accumulation [33, 80, 82].

Here, we demonstrate the presence of SNTF within damaged axons following a clinically relevant model of mTBI in a time course consistent with observations of SNTF in the serum of CT-negative mTBI patients and sports-related concussion [62, 65]. Although mTBI or "concussion" is a very common clinical designation, the underlying pathophysiology has remained unresolved, which, in turn, has precluded the development of objective diagnostic tests. Nonetheless, there is increasing recognition that a key pathological substrate of mTBI is DAI [5–7, 40, 44, 81, 84]. Our data suggest that axons may be a primary source of SNTF in mTBI and provide a pathological correlate for the blood SNTF elevations that are linked mechanistically to axon degeneration [80]. Notably, no SNTF was observed in the neuronal somata or any other cell type at any experimental time-point post-mTBI.

The clinical relevance of observations in the swine model is supported by the direct demonstration of SNTF

◀ **Fig. 8** Baseline SMI-32 staining in a human tissue from a control case (**a**) versus following acute severe TBI (**b–c**). TBI cases demonstrate occasional scattered axons with altered morphology, including greatly swollen terminal bulbs (**b–c**). Representative examples of triple immunofluorescent labeling in human white matter with SNTF (2233) (*red*), SMI-32 (*green*) and APP (*purple*) (**d**, **e**). Typically, controls displayed no APP or SNTF positive staining, but clear baseline SMI-32 immunoreactivity was visible in normal axons (**d**). Following TBI, SMI-32 swollen profiles were few in comparison to that identified by APP or SNTF and can be difficult to interpret given the baseline staining of normal axons. Complex patterns of co-localization can be observed (**e**). SNTF frequently co-localizes with APP and more occasionally SMI-32. However, SNTF and APP profiles can be observed without co-localization with other markers (**e**). NF-68 staining in human cases demonstrated baseline staining in normal control cases (**f**) when compared to acute severe TBI cases that displayed altered morphology or occasional swollen terminal bulbs (**g**, **h**). Representative examples of triple immunofluorescent labeling in humans with SNTF (2233) (*red*), NF-68 (*green*) and APP (*purple*) (**i**, **j**). Controls displayed no APP or SNTF positive staining, but baseline NF-68 immunoreactivity was observed in normal axons (**i**). Following TBI (**j**), NF-68 swollen profiles were few in comparison to that identified by APP or SNTF. SNTF frequently co-localized with APP and only occasional co-localization with NF-68 could be observed. However, again, SNTF and APP profiles could be observed without co-localization. RMO-14 immunoreactivity demonstrating normal white matter staining in a normal control case (**k**) when compared to human cases of acute TBI which displayed altered axonal morphologies including undulations and terminal axonal bulbs (**l**, **m**). Representative examples of triple immunofluorescent labeling in humans showing SNTF (2233) (*red*), RMO-14 (*green*) and APP (*purple*) (**n–q**). Controls displayed no APP or SNTF positive staining, but clear baseline RMO-14 immunoreactivity was observed in normal axons (**n**). Following TBI (**o–q**), RMO-14 swollen profiles were observed. Notably, SNTF often co-localized with RMO-14, although they appeared to occupy different compartments within terminal axonal bulbs (**o**, **p**). There was also little overlap with between RMO-14 and APP. However, SNTF and APP profiles were observed without co-localization with any other markers (**o**, **q**). **p**, **q** show higher magnification regions from **o**. *Scale bars* **a–h**, **j**, **n**, **d** 100 μm, **e**, **k–m**, **q** 50 μm, **h** 25 μm

accumulation in humans following TBI. While the human tissue was derived from cases of severe TBI, it confirms that damaged axons are an important anatomical source of SNTF clinically. Notably, while in recent years there has been extensive efforts to develop advanced neuroimaging approaches for detecting DAI post-trauma, including in mTBI [31], there are currently no conventional non-invasive diagnostic tools capable of reliably identifying DAI, even in severe TBI. The identification of specific patho-anatomic markers of axonal degeneration such as SNTF, in both serum and injured axons, provides evidence that SNTF is a biologically plausible blood biomarker for mTBI, and lends support for the potential non-invasive diagnosis of DAI via a blood test for SNTF.

In tissue derived from both the mTBI model and from severe TBI in humans, a subset of axons was identified as SNTF positive and APP negative. Yet the abundance of APP-positive axons appeared far greater than that of SNTF positive axons in all cases. Notably, the quantification of exact numbers of injured axons using 8 μm tissue sections is challenging. In particular, when comparing the typically large APP-immunoreactive swellings to those of the small and fragmented SNTF axons, standard approaches using percentage area or profile counts have limitations with respect to providing meaningful quantification of individual axon numbers. For example, for counting profiles, swollen axons may travel in and out of plane in the same section or traverse multiple sections resulting in an inaccurate overall count. Nonetheless, given these caveats, using quantitative profile counting, we estimate that SNTF identified less pathology overall than APP.

In addition, while the number of animals examined was small, the pathology observed was clear at all time points and completely absent in controls. As such, this cohort provides compelling initial findings regarding potential mechanisms of axonal degeneration. Interestingly, SNTF appeared to detect an increased proportion of pathology in the very acute phase (6 h) when compared to later time points. In contrast, APP detected an increased proportion of pathology at 48–72 h. However, examining larger groups over a more comprehensive survival time range will be important to accurately delineate the temporal evolution of pathology.

Nonetheless, together these data indicate that while SNTF IHC is not as sensitive for the detection of transport-interrupted axons, it may identify a specific subset of pathological axons. This presents the intriguing possibility that these axons are capable of degenerating via a distinct pathway independent of transport interruption. Indeed, while there has been a focus on axonal swelling leading to degeneration, calpain-mediated proteolysis is part of the spectrum of injury that may be critical for determining outcome. Notably, the morphology of SNTF axons in our animal model was frequently different from that of APP-positive axons, being smaller in diameter and much more rarely displaying fusiform or varicose swellings, consistent with an absence of transport interruption. Interestingly, this morphology of SNTF positive axons also evolved over time. Typically axons were intact and often had an undulating appearance at 6 h, a morphology that has previously been shown to occur immediately following dynamic axonal stretch in vitro and is associated with microtubule breakage [78, 79]. However, by 3 days post-injury, SNTF positive axons developed a beaded appearance indicative of degeneration, yet many remained without noticeable swelling or APP accumulation.

Given the lack of co-localization with APP in a proportion of injured axons, further experiments were performed to examine for potential co-localization with other previously identified markers of axonal pathology. Notably, while others and we historically used NF-based markers of axonal pathology, these were largely replaced with APP

IHC upon demonstration that it can detect a greater extent of pathology at earlier time points. Nonetheless, previous work by Povlishock and colleagues indicates that cytoskeletal injury to axons can occur without transport interruption detected using APP IHC, as indicated by experimental rodent models showing neurofilament compaction in the absence of APP accumulation [38, 77]. Our findings are largely consistent with what was observed in the rodent and confirm this finding for the first time in human material. Specifically, we observed a curious pattern of co-localization between SNTF, RMO-14 and NF-68 positive axons that were APP negative. In addition, all markers could be observed independently. These data support the premise that there are at least three distinct populations of injured axons post-TBI in humans and following mTBI in swine, highlighting the complex pathophysiology of axonal degeneration. Possibly, further comparisons with additional markers including other neurofilament subtypes (e.g., phosphorylated neurofilaments) may elucidate additional distinct phenotypes. Notably, while ultrastructural analyses were not possible in this study, examination of the subcellular localization of the various markers of axonal pathology may provide additional important information regarding mechanisms of axonal degeneration.

As has been described previously, NF-68 and RMO-14 proved to be more useful markers of axonal pathology than SMI-32 in both swine and humans. Moreover, while NF-68 and RMO-14 displayed some co-localization with SNTF and APP, both markers also identified a population of injured axons distinct from those identified using both SNTF and APP, although this population was small.

An important limitation of all NF-based markers is that there is a degree of baseline staining in normal axons. As such, contrasting with SNTF, simply the presence of positive NF staining alone is not indicative of pathology. Rather the presence of pathology is dependent upon the identification of axons with an abnormal morphology, which can limit the identification of more subtle changes, e.g., a swollen axon of small diameter can look similar to a normal large diameter axon if identified in the appropriate plane of sectioning.

While the reasons that SNTF positive axons fail to display markers of transport interruption in swine are unclear, the observed rapid degeneration of SNTF positive axons by 48–72 h in mTBI may indicate a more severe form of axonal perturbation. Previous studies and the current data clearly demonstrate that there is a wide array of morphological alterations in injured axons and their degenerative courses in any given injured white matter tract [12, 28, 34, 35, 70], which may reflect the spectrum of injury severity. For example, in mild forms of axonal injury, there may not be evidence of swelling or proteolysis, but these axons may nonetheless be rendered dysfunctional due to ionic perturbations. At more moderate levels of injury, physical damage may result in axonal transport interruption and accumulation of cargoes, such as APP. This range of damage may extend from minor and potentially reversible APP accumulation, to large swellings that cause secondary disconnection. However, for the most severely injured axons, it is possible that the same marked ionic imbalance that leads to SNTF genesis also induces profound mitochondrial dysfunction and energy failure [11, 46, 47], thus preventing transport in these catastrophically injured regions. This complete failure of transport, with no opportunity for extensive protein accumulation, accompanied by calcium-mediated proteolysis may induce rapid disintegration. Potentially, SNTF may be a marker for this severe form of axonal damage.

While the severity of injury to axons is dependent on the mechanics of trauma [21, 35, 43, 73], it is also possible that individual axons have selective vulnerability to mechanical injury due to their inherent structural or physiological properties. It will be of interest to further elucidate whether factors such as myelination status and caliber, previously shown to influence vulnerability to injury [52, 75], are significant in determining SNTF positivity. Understanding the differential responses of axons to trauma will provide potentially novel approaches to developing targeted interventions.

Notably, the morphological differences between SNTF and APP immunoreactivity were less apparent in human tissue following severe TBI, which displayed a wide range of SNTF positive axonal morphologies, including both small and large diameter axons, as well terminal bulbs and fusiform profiles. The reasons for the morphological differences between the mTBI model and severe TBI in humans likely reflect the much more complex, heterogeneous and evolving axonal pathologies following severe TBI in humans. Indeed, the swine model at the head rotational levels used in this study produces a very pure diffuse axonal pathology in a biomechanical distribution, without comorbid hemorrhagic or focal lesions, brain swelling or raised ICP. Severe TBI in humans often results in axonal pathology with complex, variable morphologies with differing distributions when identified using APP IHC [34, 35]. Notably, prolonged ischemia or brain swelling due to non-traumatic etiologies can also result in this pattern of APP-immunoreactive axonal pathology and has been observed in approximately 20 % of non-selected post-mortem cases without TBI [34].

The observation that SNTF can be observed relatively acutely post-trauma (within hours) suggests that it is likely accumulating at the site of mechanical injury. However, the more mixed pattern of overlap with APP and more complex overall pattern and distributions in human severe TBI indicate that SNTF reactivity can occur via multiple mechanisms, possibly independent of traumatic forces and

likely downstream from multiple mechanisms of calcium dysregulation. Nonetheless, utilizing SNTF as a marker of axonal injury in combination with APP and neurofilament subtypes clearly identified a greater extent of pathology than either marker alone, indicating potential utility in the clinical neuropathological assessment of axonal pathology.

Here we present data that provide an important anatomic and mechanistic substrate for SNTF as a clinically relevant biomarker of axonal injury. In addition, in tissue derived from both the mTBI model and post-mortem cases of TBI, the combined use of IHC specific for SNTF, APP and neurofilament subtypes offers a more comprehensive assessment of DAI.

Acknowledgments This work was supported by National Institutes of Health grants NS056202 (D.H. Smith and R. Siman), NS038104 (D.H. Smith), NS092389 (D.H. Smith), the US Department of Defense Grant PT110785 (D.H. Smith) and the NHS Research Scotland Career Research Fellowship (W. Stewart). We would like to thank Dr. John Wolf and Michael Grovola for their assistance with confocal imaging.

Compliance with ethical standards

Conflict of interest Dr. Siman is listed as inventor on patent applications for SNTF as a blood biomarker for concussion. All other authors declare that they have no conflict of interest.

Ethical approvals All applicable international, national, and/or institutional guidelines for the care and use of animals were followed. All procedures performed in studies involving human participants were in accordance with the ethical standards of the institutional and/or national research committee and with the 1964 Helsinki declaration and its later amendments or comparable ethical standards. For this type of study, formal consent is not required.

References

1. Adams JH, Doyle D, Ford I, Gennarelli TA, Graham DI, McLellan DR (1989) Diffuse axonal injury in head injury: definition, diagnosis and grading. Histopathology 15:49–59
2. Adams JH, Graham DI, Gennarelli TA, Maxwell WL (1991) Diffuse axonal injury in non-missile head injury. J Neurol Neurosurg Psychiatry 54:481–483
3. Adams JH, Graham DI, Murray LS, Scott G (1982) Diffuse axonal injury due to nonmissile head injury in humans: an analysis of 45 cases. Ann Neurol 12:557–563
4. Baines AJ (2009) Evolution of spectrin function in cytoskeletal and membrane networks. Biochem Soc Trans 37:796–803
5. Bazarian JJ, Zhong J, Blyth B, Zhu T, Kavcic V, Peterson D (2007) Diffusion tensor imaging detects clinically important axonal damage after mild traumatic brain injury: a pilot study. J Neurotrauma 24:1447–1459
6. Blumbergs PC, Scott G, Manavis J, Wainwright H, Simpson DA, McLean AJ (1994) Staining of amyloid precursor protein to study axonal damage in mild head injury. Lancet 344:1055–1056
7. Blumbergs PC, Scott G, Manavis J, Wainwright H, Simpson DA, McLean AJ (1995) Topography of axonal injury as defined by amyloid precursor protein and the sector scoring method in mild and severe closed head injury. J Neurotrauma 12:565–572
8. Browne KD, Chen XH, Meaney DF, Smith DH (2011) Mild traumatic brain injury and diffuse axonal injury in swine. J Neurotrauma 28:1747–1755
9. Buki A, Farkas O, Doczi T, Povlishock JT (2003) Preinjury administration of the calpain inhibitor MDL-28170 attenuates traumatically induced axonal injury. J Neurotrauma 20:261–268
10. Buki A, Koizumi H, Povlishock JT (1999) Moderate posttraumatic hypothermia decreases early calpain-mediated proteolysis and concomitant cytoskeletal compromise in traumatic axonal injury. Exp Neurol 159:319–328
11. Buki A, Okonkwo DO, Povlishock JT (1999) Postinjury cyclosporin A administration limits axonal damage and disconnection in traumatic brain injury. J Neurotrauma 16:511–521
12. Buki A, Povlishock JT (2006) All roads lead to disconnection?–Traumatic axonal injury revisited. Acta Neurochir (Wien) 148:181–193 (**discussion 193–184**)
13. Buki A, Siman R, Trojanowski JQ, Povlishock JT (1999) The role of calpain-mediated spectrin proteolysis in traumatically induced axonal injury. J Neuropathol Exp Neurol 58:365–375
14. Campbell MJ, Morrison JH (1989) Monoclonal antibody to neurofilament protein (SMI-32) labels a subpopulation of pyramidal neurons in the human and monkey neocortex. J Comp Neurol 282:191–205
15. Christman CW, Salvant JB Jr, Walker SA, Povlishock JT (1997) Characterization of a prolonged regenerative attempt by diffusely injured axons following traumatic brain injury in adult cat: a light and electron microscopic immunocytochemical study. Acta Neuropathol 94:329–337
16. Coronado VG, McGuire LC, Sarmiento K, Bell J, Lionbarger MR, Jones CD, Geller AI, Khoury N, Xu L (2012) Trends in traumatic brain injury in the US and the public health response: 1995–2009. J Saf Res 43:299–307
17. Eierud C, Craddock RC, Fletcher S, Aulakh M, King-Casas B, Kuehl D, LaConte SM (2014) Neuroimaging after mild traumatic brain injury: review and meta-analysis. NeuroImage Clin 4:283–294
18. Faul M, Xu L, Wald MM, Coronado VG (2010) Traumatic brain injury in the United States: emergency department visits, hospitalizations, and deaths. Centers for Disease Control and Prevention, National Center for Injury Prevention and Control, Atlanta
19. Geddes JF, Vowles GH, Beer TW, Ellison DW (1997) The diagnosis of diffuse axonal injury: implications for forensic practice. Neuropathol Appl Neurobiol 23:339–347
20. Geddes JF, Whitwell HL, Graham DI (2000) Traumatic axonal injury: practical issues for diagnosis in medicolegal cases. Neuropathol Appl Neurobiol 26:105–116
21. Gennarelli TA, Thibault LE, Adams JH, Graham DI, Thompson CJ, Marcincin RP (1982) Diffuse axonal injury and traumatic coma in the primate. Ann Neurol 12:564–574
22. Gentleman SM, Nash MJ, Sweeting CJ, Graham DI, Roberts GW (1993) Beta-amyloid precursor protein (beta APP) as a marker for axonal injury after head injury. Neurosci Lett 160:139–144
23. Gentleman SM, Roberts GW, Gennarelli TA, Maxwell WL, Adams JH, Kerr S, Graham DI (1995) Axonal injury: a universal consequence of fatal closed head injury? Acta Neuropathol 89:537–543
24. Grady MS, McLaughlin MR, Christman CW, Valadka AB, Fligner CL, Povlishock JT (1993) The use of antibodies targeted against the neurofilament subunits for the detection of diffuse axonal injury in humans. J Neuropathol Exp Neurol 52:143–152
25. Graham DI, Adams JH, Nicoll JA, Maxwell WL, Gennarelli TA (1995) The nature, distribution and causes of traumatic brain injury. Brain Pathol 5:397–406

26. Graham DI, Gentleman SM, Lynch A, Roberts GW (1995) Distribution of beta-amyloid protein in the brain following severe head injury. Neuropathol Appl Neurobiol 21:27–34
27. Graham DI, Smith C, Reichard R, Leclercq PD, Gentleman SM (2004) Trials and tribulations of using beta-amyloid precursor protein immunohistochemistry to evaluate traumatic brain injury in adults. Forensic Sci Int 146:89–96
28. Hanell A, Greer JE, McGinn MJ, Povlishock JT (2015) Traumatic brain injury-induced axonal phenotypes react differently to treatment. Acta Neuropathol 129:317–332
29. Hayashi T, Ago K, Ago M, Ogata M (2009) Two patterns of beta-amyloid precursor protein (APP) immunoreactivity in cases of blunt head injury. Leg Med (Tokyo) 11(Suppl 1):S171–S173
30. Humphreys I, Wood RL, Phillips CJ, Macey S (2013) The costs of traumatic brain injury: a literature review. ClinicoEconomics Outcomes Res: CEOR 5:281–287
31. Hunter JV, Wilde EA, Tong KA, Holshouser BA (2012) Emerging imaging tools for use with traumatic brain injury research. J Neurotrauma 29:654–671
32. Hyder AA, Wunderlich CA, Puvanachandra P, Gururaj G, Kobusingye OC (2007) The impact of traumatic brain injuries: a global perspective. NeuroRehabilitation 22:341–353
33. Iwata A, Stys PK, Wolf JA, Chen XH, Taylor AG, Meaney DF, Smith DH (2004) Traumatic axonal injury induces proteolytic cleavage of the voltage-gated sodium channels modulated by tetrodotoxin and protease inhibitors. J Neurosci 24:4605–4613
34. Johnson VE, Stewart JE, Begbie FD, Trojanowski JQ, Smith DH, Stewart W (2013) Inflammation and white matter degeneration persist for years after a single traumatic brain injury. Brain 136:28–42
35. Johnson VE, Stewart W, Smith DH (2013) Axonal pathology in traumatic brain injury. Exp Neurol 246:35–43
36. Kampfl A, Posmantur R, Nixon R, Grynspan F, Zhao X, Liu SJ, Newcomb JK, Clifton GL, Hayes RL (1996) mu-Calpain activation and calpain-mediated cytoskeletal proteolysis following traumatic brain injury. J Neurochem 67:1575–1583
37. Leclercq PD, McKenzie JE, Graham DI, Gentleman SM (2001) Axonal injury is accentuated in the caudal corpus callosum of head-injured patients. J Neurotrauma 18:1–9
38. Marmarou CR, Walker SA, Davis CL, Povlishock JT (2005) Quantitative analysis of the relationship between intra- axonal neurofilament compaction and impaired axonal transport following diffuse traumatic brain injury. J Neurotrauma 22:1066–1080
39. Maxwell WL, Watt C, Pediani JD, Graham DI, Adams JH, Gennarelli TA (1991) Localisation of calcium ions and calcium-ATPase activity within myelinated nerve fibres of the adult guinea-pig optic nerve. J Anat 176:71–79
40. Mayer AR, Ling J, Mannell MV, Gasparovic C, Phillips JP, Doezema D, Reichard R, Yeo RA (2010) A prospective diffusion tensor imaging study in mild traumatic brain injury. Neurology 74:643–650
41. McCracken E, Hunter AJ, Patel S, Graham DI, Dewar D (1999) Calpain activation and cytoskeletal protein breakdown in the corpus callosum of head-injured patients. J Neurotrauma 16:749–761
42. McGinn MJ, Kelley BJ, Akinyi L, Oli MW, Liu MC, Hayes RL, Wang KK, Povlishock JT (2009) Biochemical, structural, and biomarker evidence for calpain-mediated cytoskeletal change after diffuse brain injury uncomplicated by contusion. J Neuropathol Exp Neurol 68:241–249
43. Meaney DF, Smith DH, Shreiber DI, Bain AC, Miller RT, Ross DT, Gennarelli TA (1995) Biomechanical analysis of experimental diffuse axonal injury. J Neurotrauma 12:689–694
44. Miles L, Grossman RI, Johnson G, Babb JS, Diller L, Inglese M (2008) Short-term DTI predictors of cognitive dysfunction in mild traumatic brain injury. Brain Inj 22:115–122
45. Niogi SN, Mukherjee P, Ghajar J, Johnson C, Kolster RA, Sarkar R, Lee H, Meeker M, Zimmerman RD, Manley GT et al (2008) Extent of microstructural white matter injury in postconcussive syndrome correlates with impaired cognitive reaction time: a 3T diffusion tensor imaging study of mild traumatic brain injury. AJNR Am J Neuroradiol 29:967–973
46. Okonkwo DO, Melon DE, Pellicane AJ, Mutlu LK, Rubin DG, Stone JR, Helm GA (2003) Dose-response of cyclosporin A in attenuating traumatic axonal injury in rat. NeuroReport 14:463–466
47. Okonkwo DO, Povlishock JT (1999) An intrathecal bolus of cyclosporin A before injury preserves mitochondrial integrity and attenuates axonal disruption in traumatic brain injury. J Cereb Blood Flow Metab 19:443–451
48. Pettus EH, Christman CW, Giebel ML, Povlishock JT (1994) Traumatically induced altered membrane permeability: its relationship to traumatically induced reactive axonal change. J Neurotrauma 11:507–522
49. Pettus EH, Povlishock JT (1996) Characterization of a distinct set of intra-axonal ultrastructural changes associated with traumatically induced alteration in axolemmal permeability. Brain Res 722:1–11
50. Povlishock JT, Buki A, Koiziumi H, Stone J, Okonkwo DO (1999) Initiating mechanisms involved in the pathobiology of traumatically induced axonal injury and interventions targeted at blunting their progression. Acta Neurochir Suppl 73:15–20
51. Povlishock JT, Marmarou A, McIntosh T, Trojanowski JQ, Moroi J (1997) Impact acceleration injury in the rat: evidence for focal axolemmal change and related neurofilament sidearm alteration. J Neuropathol Exp Neurol 56:347–359
52. Reeves TM, Phillips LL, Povlishock JT (2005) Myelinated and unmyelinated axons of the corpus callosum differ in vulnerability and functional recovery following traumatic brain injury. Exp Neurol 196:126–137
53. Reichard RR, Smith C, Graham DI (2005) The significance of beta-APP immunoreactivity in forensic practice. Neuropathol Appl Neurobiol 31:304–313
54. Roberts-Lewis JM, Savage MJ, Marcy VR, Pinsker LR, Siman R (1994) Immunolocalization of calpain I-mediated spectrin degradation to vulnerable neurons in the ischemic gerbil brain. J Neurosci: Off J Soc Neurosci 14:3934–3944
55. Ross DT, Meaney DF, Sabol MK, Smith DH, Gennarelli TA (1994) Distribution of forebrain diffuse axonal injury following inertial closed head injury in miniature swine. Exp Neurol 126:291–299
56. Saatman KE, Abai B, Grosvenor A, Vorwerk CK, Smith DH, Meaney DF (2003) Traumatic axonal injury results in biphasic calpain activation and retrograde transport impairment in mice. J Cereb Blood Flow Metab 23:34–42
57. Saatman KE, Bozyczko-Coyne D, Marcy V, Siman R, McIntosh TK (1996) Prolonged calpain-mediated spectrin breakdown occurs regionally following experimental brain injury in the rat. J Neuropathol Exp Neurol 55:850–860
58. Shahim P, Tegner Y, Wilson DH, Randall J, Skillback T, Pazooki D, Kallberg B, Blennow K, Zetterberg H (2014) Blood biomarkers for brain injury in concussed professional ice hockey players. JAMA neurol 71:684–692
59. Sherriff FE, Bridges LR, Sivaloganathan S (1994) Early detection of axonal injury after human head trauma using immunocytochemistry for beta-amyloid precursor protein. Acta Neuropathol (Berl) 87:55–62
60. Shoji M, Golde TE, Ghiso J, Cheung TT, Estus S, Shaffer LM, Cai XD, McKay DM, Tintner R, Frangione B et al (1992) Production of the Alzheimer amyloid beta protein by normal proteolytic processing. Science 258:126–129

61. Siman R, Flood DG, Thinakaran G, Neumar RW (2001) Endoplasmic reticulum stress-induced cysteine protease activation in cortical neurons: effect of an Alzheimer's disease-linked presenilin-1 knock-in mutation. J Biol Chem 276:44736–44743
62. Siman R, Giovannone N, Hanten G, Wilde EA, McCauley SR, Hunter JV, Li X, Levin HS, Smith DH (2013) Evidence that the blood biomarker SNTF predicts brain imaging changes and persistent cognitive dysfunction in mild TBI patients. Frontiers in neurology 4:190
63. Siman R, McIntosh TK, Soltesz KM, Chen Z, Neumar RW, Roberts VL (2004) Proteins released from degenerating neurons are surrogate markers for acute brain damage. Neurobiol Dis 16:311–320
64. Siman R, Noszek JC, Kegerise C (1989) Calpain I activation is specifically related to excitatory amino acid induction of hippocampal damage. J Neurosci 9:1579–1590
65. Siman R, Shahim P, Tegner Y, Blennow K, Zetterberg H, Smith DH (2015) Serum SNTF increases in concussed professional ice hockey players and relates to the severity of postconcussion symptoms. J Neurotrauma (**in press**)
66. Siman R, Toraskar N, Dang A, McNeil E, McGarvey M, Plaum J, Maloney E, Grady MS (2009) A panel of neuron-enriched proteins as markers for traumatic brain injury in humans. J Neurotrauma 26:1867–1877
67. Siman R, Zhang C, Roberts VL, Pitts-Kiefer A, Neumar RW (2005) Novel surrogate markers for acute brain damage: cerebrospinal fluid levels corrrelate with severity of ischemic neurodegeneration in the rat. J Cereb Blood Flow Metab: Off J Int Soc Cereb Blood Flow Metab 25:1433–1444
68. Singleton RH, Stone JR, Okonkwo DO, Pellicane AJ, Povlishock JT (2001) The immunophilin ligand FK506 attenuates axonal injury in an impact-acceleration model of traumatic brain injury. J Neurotrauma 18:607–614
69. Smith DH, Chen XH, Xu BN, McIntosh TK, Gennarelli TA, Meaney DF (1997) Characterization of diffuse axonal pathology and selective hippocampal damage following inertial brain trauma in the pig. J Neuropathol Exp Neurol 56:822–834
70. Smith DH, Hicks R, Povlishock JT (2013) Therapy development for diffuse axonal injury. J Neurotrauma 30:307–323
71. Smith DH, Johnson VE, Stewart W (2013) Chronic neuropathologies of single and repetitive TBI: substrates of dementia? Nat Rev Neurol 9:211–221
72. Smith DH, Nonaka M, Miller R, Leoni M, Chen XH, Alsop D, Meaney DF (2000) Immediate coma following inertial brain injury dependent on axonal damage in the brainstem. J Neurosurg 93:315–322
73. Smith DH, Wolf JA, Lusardi TA, Lee VM, Meaney DF (1999) High tolerance and delayed elastic response of cultured axons to dynamic stretch injury. J Neurosci 19:4263–4269
74. Staal JA, Dickson TC, Gasperini R, Liu Y, Foa L, Vickers JC (2010) Initial calcium release from intracellular stores followed by calcium dysregulation is linked to secondary axotomy following transient axonal stretch injury. J Neurochem 112:1147–1155
75. Staal JA, Vickers JC (2011) Selective vulnerability of non-myelinated axons to stretch injury in an in vitro co-culture system. J Neurotrauma 28:841–847
76. Sternberger LA, Sternberger NH (1983) Monoclonal antibodies distinguish phosphorylated and nonphosphorylated forms of neurofilaments in situ. Proc Natl Acad Sci USA 80:6126–6130
77. Stone JR, Singleton RH, Povlishock JT (2001) Intra-axonal neurofilament compaction does not evoke local axonal swelling in all traumatically injured axons. Exp Neurol 172:320–331
78. Tang-Schomer MD, Johnson VE, Baas PW, Stewart W, Smith DH (2012) Partial interruption of axonal transport due to microtubule breakage accounts for the formation of periodic varicosities after traumatic axonal injury. Exp Neurol 233:364–372
79. Tang-Schomer MD, Patel AR, Baas PW, Smith DH (2010) Mechanical breaking of microtubules in axons during dynamic stretch injury underlies delayed elasticity, microtubule disassembly, and axon degeneration. FASEB J 24:1401–1410
80. von Reyn CR, Spaethling JM, Mesfin MN, Ma M, Neumar RW, Smith DH, Siman R, Meaney DF (2009) Calpain mediates proteolysis of the voltage-gated sodium channel alpha-subunit. J Neurosci 29:10350–10356
81. Wilde EA, McCauley SR, Hunter JV, Bigler ED, Chu Z, Wang ZJ, Hanten GR, Troyanskaya M, Yallampalli R, Li X et al (2008) Diffusion tensor imaging of acute mild traumatic brain injury in adolescents. Neurology 70:948–955
82. Wolf JA, Stys PK, Lusardi T, Meaney D, Smith DH (2001) Traumatic axonal injury induces calcium influx modulated by tetrodotoxin-sensitive sodium channels. J Neurosci 21:1923–1930
83. Yaghmai A, Povlishock J (1992) Traumatically induced reactive change as visualized through the use of monoclonal antibodies targeted to neurofilament subunits. J Neuropathol Exp Neurol 51:158–176
84. Yallampalli R, Wilde EA, Bigler ED, McCauley SR, Hanten G, Troyanskaya M, Hunter JV, Chu Z, Li X, Levin HS (2013) Acute white matter differences in the fornix following mild traumatic brain injury using diffusion tensor imaging. J Neuroimaging: Off J Am Soc Neuroimaging 23:224–227
85. Yamazaki T, Koo EH, Selkoe DJ (1997) Cell surface amyloid beta-protein precursor colocalizes with beta 1 integrins at substrate contact sites in neural cells. J Neurosci 17:1004–1010